A Jasmonate signaling network activates root stem cells and promotes regeneration

Wenkun Zhou[1,2], Jose L. Lozano-Torres[3], Ikram Blilou[1,4], Xiaoyue Zhang[2], Qingzhe Zhai[2], Geert Smant[3], Chuanyou Li[2], Ben Scheres[1,5,6,*]

[1]Laboratory of Plant Developmental Biology, Wageningen University Research, 6708 PB Wageningen, the Netherlands.

[2]State Key Laboratory of Plant Genomics and National Center for Plant Gene Research (Beijing), Institute of Genetics and Developmental Biology, Chinese Academy of Sciences, Beijing 100101, China.

[3]Laboratory of Nematology, Wageningen University Research, 6708 PB Wageningen, the Netherlands.

[4]KAUST, Thuwall 23955, Saudi Arabia

[5]Rijk Zwaan R&D, 4793 RS Fijnaart, The Netherlands.

[6]Lead Contact

*Correspondence, ben.scheres@wur.nl

Abstract

Plants are sessile and have to cope with environmentally induced damage through modification of growth and defense pathways. It is an open question how tissue regeneration is triggered in such responses and whether this involves stem cell activation. The stress hormone jasmonate (JA) plays well-established roles in wounding and defense responses. JA also affects growth which is hitherto interpreted as trade-off between growth and defense. Here, we describe a molecular network triggered by wound-induced JA that promotes stem cell activation and regeneration. JA regulates organizer cell activity in the root stem cell niche through the RBR-SCR network and stress response protein ERF115. Moreover, JA-induced ERF109 transcription stimulates *CYCD6;1* expression, functions upstream of ERF115 and promotes regeneration. Soil penetration and response to nematode herbivory induce and require this JA mediated regeneration response. Therefore, the JA tissue damage response pathway induces stem cell activation and regeneration, and activates growth after environmental stress.

Introduction

Plants are sessile and respond to environmental challenges by reallocating resources between growth, response to abiotic stress, and defense. This reallocation results from the convergence of developmental and environmental signaling networks; the response pathway to stress-induced hormones jasmonate (JA), salicylic acid, abscisic acid and ethylene influence plant growth by interacting with signaling pathways that respond to growth signals like gibberellin, brassinolide and auxin in regions of plant growth (Campos et al., 2016; Chen et al., 2004; Hou et al., 2010; Nemhauser et al., 2006). The negative growth control by defense signaling is thought to ensure a proper resource cost trade-off (Karasov et al., 2017). However, plants can also positively regulate growth after physical damage caused by abiotic or biotic insults, to regenerate tissues or even complete organs (Sena et al., 2009; Sugimoto et al., 2010; Xu et al., 2006). Regeneration responses correlate with growth signaling (Efroni et al., 2016; Ikeuchi et al., 2017; Ikeuchi et al., 2018; Kareem et al., 2015; Melnyk et al., 2018; Sugimoto et al., 2010; Xu et al., 2006). It has however not been clarified how physical stress or damage triggers local regeneration responses.

The stress hormone JA, structurally similar to the animal defense regulator prostaglandin (Mueller, 1998), is a candidate trigger for regeneration responses. JA plays well-established roles in defense responses against necrotrophic pathogens and insect herbivores, and also in abiotic stress responses, reproductive development, and metabolism (Pieterse et al., 2012; Yang et al., 2012; Yan et al., 2018). JA rapidly accumulates after damage and pathogen detection cues (Glauser et al., 2009; Larrieu et al., 2015; Wasternack and Hause, 2013). Several studies have implicated JA in *in vitro* tissue regeneration, e.g. (Asahina et al., 2011; Ikeuchi et al., 2017). It is unknown whether JA regulates only biochemical defense and global growth regulation or also organ regeneration after *in vivo* insult. F-box protein CORONATINE INSENSITIVE1 (COI1), and the jasmonate ZIM domain (JAZ) repressor proteins act as JA co-receptors (Sheard et al., 2010; Yan et al., 2009). Upon JA perception, JAZ proteins are targeted by COI1 for degradation, which de-represses transcription factors like MYC2 and induces JA-responsive gene expression (Dombrecht et al., 2007; Hickman et al., 2017; Zhang et al., 2015a).

Continuous cell production plant meristems is maintained by stem cells, and by analogy to animal models stem cell activation may be a significant factor in wounding-triggered regeneration. In the model plant *Arabidopsis thaliana*, root stem cells include mitotically less active organizer cells called the quiescent centre (QC) and the surrounding initials, which together form the root stem cell niche (Cruz-Ramirez et al., 2013) (Figure S1A). Stress hormones JA, abscisic acid and ethylene can regulate the division rate of organizer cells suggesting that stem cell activation may take part in regeneration responses (Chen et al., 2011; Zhang et al., 2010; Ortega-Martínez et al., 2007). The RETINOBLASTOMA-RELATED (RBR)-SCARECROW (SCR) –SHORT ROOT (SHR) protein network regulates asymmetric cell divisions of root stem cells, QC quiescence and the activation of the QC regulatory protein WOX5 (Cruz-Ramirez et al., 2012; Cruz-Ramirez et al., 2013; Shimotohno et al., 2018). RBR binds and regulates the activity of SHR-SCR in a network together with the growth hormone auxin and the CDK interactor *CYCLIND6;1* (*CYCD6;1*) in ground tissue initials (Cruz-Ramirez et al., 2012). In addition, RBR reinforces mitotic quiescence in the QC. Disruption of the RBR-SCR interaction by point mutations in SCR (*pSCR::SCRaca-YFP*) or QC-specific knockdown of RBR (*pWOX5::amiGORBR*) promotes QC divisions (Cruz-Ramirez et al., 2013). In addition, the AP2/ERF subfamily X transcription factors ERF109 and ERF115 have been reported to maintain QC quiescence in unperturbed conditions (Heyman et al., 2013; Heyman et al., 2017; Kong et al., 2018). ERF115 activity is required for wounding-induced regeneration responses in roots (Heyman et al., 2016).

Here, we reveal that stress hormone JA reduces QC quiescence through the previously established RBR-SCR and ERF115 pathways. JA-induced ERF109 transcription stimulates *CYCD6;1* expression, functions upstream of ERF115 and promotes regeneration. RBR-SCR operates downstream of ERF115 both in stem cell regulation and in tissue regeneration. JA and auxin synergistically activate these regeneration regulators. Finally, soil penetration and nematode herbivory activate this molecular regeneration network.

Results

JA acts through RBR-SCR to regulate quiescence

We confirmed that JA promotes division of QC cells (Chen et al., 2011) (Figures 1A and 1B, S1B and S1C), and that extra QC divisions occur in plants with altered SCR-RBR network: *pWOX5::amiGORBR*, which specifically downregulates RBR in the QC, and *pSCR::SCRaca-YFP*, which specifically disrupts RBR-SCR protein interaction (Cruz-Ramirez et al., 2013) (Figures 1D and 1G). We observed QC divisions in wild type Col-0 after 50 µM or 100 µM MeJA (methyl ester of JA) treatment for 48 hours (Figures 1A-1C and 1J), respectively. Conversely, no extra QC divisions were detected in *pWOX5::amiGORBR* and *pSCR::SCRaca-YFP* lines treated with 50 µM or 100 µM MeJA for the same period (Figures 1D-1I and 1K-1L), suggesting that JA may function through the SCR-RBR network in regulating quiescence of QC. To further confirm this, we introgressed the JA receptor loss of function mutant allele *coi1-2* (Xu et al., 2002) into *pWOX5::amiGORBR* and *pSCR::SCRaca-YFP* lines. The QC division phenotypes and QC cell numbers of these introgression lines revealed no differences to *pSCR::SCRaca-YFP* and *pWOX5::amiGORBR* lines, both with and without MeJA treatment, respectively (Figures S1D-S1M). These findings position SCR and RBR downstream of COI1 to control quiescence of QC. After MeJA treatment, QC cell numbers of *scr-3* and *shr-2* mutants did not increase significantly compared to controls (Figures S1N-S1T), confirming that JA induces QC division through the SCR/SHR pathway. *SCR* and *RBR* expression levels were not altered significantly after MeJA treatment, judged by marker expression and reverse transcription-quantitative polymerase chain reaction (RT-qPCR) assays (Figures S1U-S1AA). These data indicate that JA does not regulate *SCR* and *RBR* at the gene expression level.

JA directly induces *ERF115* transcription

The AP2/ERF family transcription factor ERF115 was reported to control root QC cell division (Heyman et al., 2013). When *35S::ERF115* (hereafter, *ERF115-OE*), *35S::ERF115-SRDX* (hereafter, *ERF115-SRDX*, a dominant negative form of ERF115 fused with the SUPERMAN repression domain) and *erf115* knockout mutant were treated with MeJA, no extra QC divisions occurred in *ERF115-OE* and *ERF115-SRDX* compared to mock treatment. *erf115* showed reduced JA-mediated QC divisions compared to Col-0 (Figures 2A-2E, S2A), indicating that JA cannot bypass ERF115 function in regulating QC quiescence.

ERF115 promoter activity was induced by MeJA (Figures 2F-2L). Up-regulation of *ERF115* was first detected after 1 hour of MeJA treatment in vascular protoxylem cells (Figures S2B and S2C), and induction was additionally observed in QC cells after longer treatment (Figures 2F-2L). RT-qPCR assays showed JA mediated *ERF115* transcript induction, which was reduced in the *myc2-2* mutant (Boter et al., 2004) and largely diminished in the JA receptor mutant *coi1-2* (Figure 2M), suggesting that JA induces *ERF115* in a COI1- and MYC2-dependent manner. MYC2 preferably binds to the G-box-related hexamer (5'-CACGTG-3') in promoters of its target genes (Dombrecht et al., 2007), and we identified one such motif in the promoter of *ERF115* (-1482 bp to -1476 bp) (Figure 2N). Chromatin immunoprecipitation-quantitative PCR (ChIP-qPCR) assays using MYC2-GFP plants and anti-GFP antibodies revealed enrichment of MYC2 in a region approximately 1,500 bp upstream of the *ERF115* promoter, covering the identified G-box motif (Figure 2O). We generated *pERF115::GUS* lines as control and *pmERF115::GUS* lines in which the G-box was mutated to 5'-AAAAAA-3' (Figure 2P). In accordance with a crucial role for the identified G-box, JA induction of *ERF115* in QC and vascular cells was almost abolished in *pmERF115::GUS* lines, and only sporadic induction was observed in a few vascular cells (Figure 2Q). These findings together indicate that *ERF115* is induced by JA and is a direct target of MYC2.

Reactive oxygen species (ROS) and brassinosteroids (BR) also regulate QC quiescence and expression of *ERF115* (Heyman et al., 2013; Kong et al., 2018; Vilarrasa-Blasi et al., 2014). We explored whether these signals converge with JA. *coi1-2* was responsive to BR-mediated QC division and *ERF115* induction (Figures S2D and S2E), suggesting parallel input of BR and JA in QC quiescence and *ERF115* induction. *coi1-2* was also responsive to ROS-mediated QC division (Figure S2F), but ROS-mediated *ERF115* induction was reduced in *coi1-2* compared to WT (Figure S2G), indicating that ROS and JA partially converge in regulating *ERF115* expression.

SCR-RBR connects ERF115 activation to regulating QC quiescence

As SCR-RBR and ERF115 act downstream of JA to regulate QC quiescence, we examined potential genetic interactions between SCR-RBR and ERF115. We combined *pWOX5::amiGORBR* and *pSCR::SCRaca-YFP* lines with both *ERF115-OE* and *ERF115-SRDX* lines. In contrast to *ERF115-SRDX* lines, which seldom displayed QC divisions at 6 days after germination (DAG), both *pSCR::SCRaca-YFP ERF115-SRDX* and *pWOX5::amiGORBR ERF115-SRDX* lines revealed a decrease in QC quiescence, approaching the QC phenotypes of *pSCR::SCRaca-YFP* and *pWOX5::amiGORBR*, respectively (Figures 3A-3K and S3A-S3E). Quantification of QC cell numbers confirmed that both *pSCR::SCRaca-YFP ERF115-SRDX* (median QC cell number=4.5) and *pWOX5::amiGORBR ERF115-SRDX* (median QC cell number=5) similarly decreased QC quiescence compared with *pSCR::SCRaca-YFP* (median QC cell number=4) and *pWOX5::amiGORBR* (median QC cell number=6), while *ERF115-SRDX* increased QC quiescence (median QC cell number=2.5) compared with *pWOX5::amiGORBR* and *pSCR::SCRaca-YFP* (Figure 3K). The observed epistasis of SCR-RBR network mutant phenotypes over ERF115 phenotypes in regulation of quiescence positions SCR-RBR downstream of ERF115 activity.

RBR can interact with proteins containing the LxCxE (Leu-x-Cys-x-Glu) motif (Cruz-Ramirez et al., 2012; reviewed in Dick, 2007). We identified a related motif (LxFxE), which was reported to bind to Rb (Retinoblastoma) in animals (Kehn et al., 2005), in the AP2 domain of ERF115 (Figure S3F). RBR and ERF115 interacted in yeast two hybrid, in planta split-YFP and co-immunoprecipitation assays (Figures S3G-S3I). We mutated the LxFxE motif into AxAxA (Ala-x-Ala-x-Ala, ERF115m), and still observed interactions between RBR and ERF115m (Figures S3G and S3H), indicating that the LxFxE motif is not essential for interaction and RBR may also bind to other ERF115 residues. The physical interaction between ERF115 and RBR suggests that JA-induced ERF115 may directly regulate RBR activity. ERF115-SRDX retains the capacity to bind to RBR (Figure S3H and S3I), suggesting a mechanism whereby ERF115 inhibits RBR activity (that inhibits SCR activity). ERF115-OE in this scenario inhibits RBR repression of SCR which activates QC division; RBR-SCR-recruited ERF115-SRDX represses transcription of SCR targets through its SRDX motif, which inhibits QC division (Figure 3L). The effect of RBR and ERF115 on QC cell number is larger than the SCR effect indicating that these two factors also act independently of SCR in regulating QC quiescence (Figure 3L).

JA signaling promotes stem cell niche regeneration

W asked whether the JA-mediated stimulation of QC division might be part of a wounding response and/or a regeneration response after damage. To monitor QC divisions after local wounding we performed laser ablation experiments (Xu et al., 2006) to ablate columella stem cells (CSCs), which are the distal neighbours of QC cells. Indeed, we observed replenishment of these cells by QC cells over time (Figures 4A-4F). When roots were pre-treated with MeJA for 24 hours (to pre-induce ERF115) before ablation, QC cells replenished the ablated CSCs faster compared to mock treatment (Figures 4A-4G, S4A-S4B). JA pre-treatment consistently increased the number of new columella cell layers between QC and ablated cells compared to mock treatment. Also incubation on 250 nM MeJA led to increased columella cell layers between QC and ablated cells compared with mock treatment (Figures S4C-S4E). These findings suggest that JA stimulates stem cell replacement after ablation.

Ablation of the QC leads to a local regeneration response that replenishes the entire stem cell niche (Xu et al., 2006). To investigate whether impaired JA signaling impedes root stem cell niche regeneration, we performed QC laser ablation in *coi1-1* null allele (Xie et al., 1998), *coi1-2* and WT col-0 roots. A delay of stele re-programming to form a new QC (marked by WOX5-GFP) was observed in *coi1-1 pWOX5::GFP* compared to WT during the time course after ablation (Figures 4H-4K and S4F-S4G). Quantification of new columella layers between new QC and ablated cells, both upon partial and whole QC ablation, confirmed the observed delayed regeneration responses upon ablation in *coi1-1* and *coi1-2* mutants compared to WT (Figures 4L and 4M). These data indicate that JA responses enhance stem cell niche replacement.

JA quickly accumulates after mechanical wounding (Glauser et al., 2009). To measure JA response after ablation, we used the 'inverse' JA biosensor *JAS9-VENUS* (*35S::JAS9-VENUS/35S::H2B-RFP*) (Larrieu et al., 2015). Expression of *JAS9-VENUS* in WT was consistently reduced after QC ablation compared with mock, while expression of *JAS9-VENUS* in *coi1-2* was comparable between mock and after ablation (Figures 4N, S4H and S4I). As JAS9-VENUS expression is anti-correlated with JA level, our results indicate that the *in vivo* JA level increases rapidly after laser ablation and that the observed stem cell regeneration may be part of a wounding response.

As ERF115 acts downstream of JA (Figure 2), and is induced by cell death and required for root regeneration (Heyman et al., 2016), we examined the role of ERF115 in stem cell regeneration. QC ablation triggered induction of *ERF115* in WT, but significantly less in *coi1-2* compared with WT (Figures S4J-S4L). In time courses after QC ablation, *ERF115-OE pWOX5::GFP* exhibited a faster replenishment of ablated cells compared to *pWOX5::GFP*, while *erf115 pWOX5::GFP* and *ERF115-SRDX pWOX5::GFP* showed a slower replenishment compared to WT (Figures 4O-4U, S4M-S4P), indicating that ERF115 is a positive regulator for stem cell regeneration.

We examined whether SCR-RBR is also involved in stem cell regeneration. After QC ablation, new columella layers between QC and ablated cells after ablation arose at similar rate as control in *pSCR::SCRaca-YFP pWOX5::GFP/scr-4* lines (Figures S4Q-S4S). While the control revealed complete re-programming of SCR and *WOX5* expression domains, neither *SCR* nor *WOX5* was expressed in the newly regenerated "QC" cells in *pSCR::SCRaca-YFP pWOX5::GFP/scr-4* lines after ablation (Figures S4Q-S4R), indicating a defect in QC fate reprogramming when the RBR interaction motif of SCR is disrupted.

New columella layers between QC and ablated cells during the time course after ablation showed that both *ERF115-SRDX pWOX5::amiGORBR* and *ERF115-SRDX pSCR::SCRaca-YFP* significantly rescued the regeneration defect of *ERF115-SRDX* (Figures S4T-S4Y), consistent with our earlier data indicating that RBR-SCR acts downstream of ERF115 in the control of QC cell division. However, the regeneration speed was still slower when compared to *pWOX5::amiGORBR* and *pSCR::SCRaca-YFP* lines (Figures S4T and S4Y). Therefore, during stem cell niche regeneration, the *ERF115-SRDX* effects are significantly but not completely mediated by the QC expressed SCR-RBR complex, indicating that ERF115 does not exclusively act on SCR regulated genes in this process (Figure 4V).

ERF109 responds quickly to JA and wounding, and is required for tissue regeneration

ERF115 is required for root tissue regeneration after resection (Heyman et al., 2016), which provokes a more dramatic regeneration response than local laser ablations (Sena et al., 2009). In addition, knockdown of *RBR* (*35S::amiGORBR*) showed enhanced tissue regeneration after resection compared with controls (Figures 5A-5C). These clues led us to further investigate the role of JA in tissue regeneration. The expression of JAS9-VENUS was lowered one minute after resection compared to uncut control, and further reduced to 25 percent of control 30 minutes after resection, while degradation of JAS9-VENUS was largely abolished in *coi1-2* mutant after root tip resection (Figures S5A-S5C), indicating that the *in vivo* JA response increases rapidly after resection. Consistently, induction of *ERF115* was largely reduced in *coi1-2* compared with Col-0, and also in *pmERF115::GUS* compared with *pERF115::GUS* after resection (Figures S5D-S5G), indicating that JA-mediated *ERF115* transcription is reduced and/or delayed when JA signaling is compromised.

As JA was induced after wounding within seconds, and *ERF115* was activated within hours, we explored potential early regulators downstream of JA. ERF109 is an ERF115 homologue, and *pERF109::GUS* can respond to JA within minutes (Cai et al., 2014; Wang et al., 2008). *pERF109::GFP* lines revealed that *ERF109* promoter activity was highly induced by MeJA also in the root stem cell niche and meristem (Figure 5D). RT-qPCR confirmed that *ERF109* mRNA was up-regulated after MeJA treatment (Figure S5H) and MYC2, MYC3 and MYC4 redundantly regulated ERF109 induction (Figure 5E). ChIP-qPCR assays further indicated that MYC2 directly binds to the promoter of *ERF109* (Figure 5F).

ERF109 was also quickly induced after laser ablation (Figures S5I) and root-tip resection (Figures 5G, 5H, S5J). This induction depends on COI1, as weaker induction was observed near the cut site 3 hours after resection in the *coi1-1 pERF109::GUS* background, compared to WT (Figure 5H). We also performed low cuts (resection site around QC) and high cuts (resection site at the elongation zone) of *pERF109::GUS* root meristems. The *ERF109* promoter was highly active in the meristem after low cuts, but less after high cuts (Figures S5K), indicating that induction of *ERF109* after resection may correlate with the regeneration capacity of remaining tissue after resection.

ERF115 mRNA was increased in the *ERF109* over-expression line (*ERF109-OE*) (Cai et al., 2014) and decreased in the *erf109* mutant (Figure 5I). On the other hand, *ERF109* was not altered significantly in either *ERF115-OE*, *ERF115-SRDX* or *erf115* mutant backgrounds (Figure 5J). In addition, JA-mediated *ERF115* induction decreased in *35S::ERF109-SRDX* compared with WT (Figures S5L and S5M). These results indicate that ERF109 acts upstream to regulate *ERF115* transcript levels. Root-tip resection experiments in *pERF109::GUS ERF115-SRDX* and *pERF109::GUS ERF115-OE* lines revealed the induction of *ERF109* was not altered in these backgrounds compared with control (Figures S5N-S5P), consistent with ERF109 acting upstream of the *ERF115* transcriptional response to wounding.

Resection experiments in *pWOX5::GFP* and *pWOX5::GFP erf109* lines revealed that the *erf109* mutant exhibited similar stem cell niche regeneration compared with WT (Figure S5Q), but an impaired capacity of tissue regeneration at categories II and III, compared to WT (Figures 5K-5M), while meristem length of unperturbed roots was comparable with WT (Figure S5R). These findings indicated that ERF109 is required for tissue regeneration. *coi1-1* and *erf115* mutants also showed a reduced frequency of regeneration after root tip resection

(Figures 5N, S5T) and similar meristem length, compared with WT (Figures S5S and S5U). *ERF115-SRDX* showed a more severe regeneration defect compared with WT (Figures S5T and S5U), suggesting functional redundancy (Heyman et al., 2016). Collectively, our data reveal a JA pathway where a wounding signal is transduced through ERF109 and ERF115 and possible redundant factors, to regulate large scale tissue regeneration (Figure 5O).

Synergy between JA and auxin signaling in regulating regeneration

How can tissue wide induction of *ERF109* by a JA triggered wounding response trigger protoxylem specific induction of *ERF115*? Auxin signaling promotes regeneration and is active in the xylem axis (Efroni et al., 2016; Xu et al., 2006), so it could restrict the induction of *ERF115* by ERF109. Indeed, we observed *ERF115* induction by auxin in protoxylem cells, and IAA together with MeJA enhanced *ERF115* promoter activity in vasculature (Figures 6A-6D). RT-qPCR assays confirmed induction of *ERF115* transcription with MeJA and IAA, respectively. Combined MeJA+IAA treatment resulted in a more-than-additive induction (Figure 6E). On the other hand, IAA did not activate root tip expression of *pERF109::GUS*, and did not significantly increase its activation by MeJA (Figures S6A and S6B). These data suggest a synergy between auxin and JA signaling in the activation of *ERF115* in protoxylem cells.

We explored other potentially tissue-specific regulators of regeneration under control of both auxin and JA. CYCD6;1, activated by SHR-SCR and auxin, is a stem cell associated regulator of RBR activity (Cruz-Ramirez et al., 2012; Sozzani et al., 2010). SCR-RBR, together with CYCD6;1, defines the position of asymmetric cell division in root stem cells (Cruz-Ramirez et al., 2012) (Figure 6M). When the *pCYCD6;1::GUS-GFP* line was treated with MeJA, *CYCD6;1* was induced along the endodermal cell layer, while it remained restricted to cortex/endodermal initials (CEI) without MeJA treatment (Figures 6F, S6C). *CYCD6;1* was also induced 3 hours after resection, and was induced ectopically after root-tip resection after 6 hours (Figures S6D-S6E). Induction culminated around 24 hours after resection and receded to the newly re-programmed CEI 48 hours after resection (Figures S6E). We conclude that *CYCD6;1* is not only induced by auxin, but also by JA and wounding.

We next investigated upstream JA-mediated regulators of *CYCD6;1*. Dual-luciferase assays in *Nicotiana benthamiana* leaves showed that ERF109 increased the activity of *pCYCD6;1::LUC* 8 fold compared with the basal level of *pCYCD6;1::LUC* alone, whereas ERF115 barely increased the activity of *pCYCD6;1::LUC* (Figure 6G). ChIP-qPCR assays revealed that ERF109 bound to the promoter of *CYCD6;1* (Figure S6F). JA-mediated *CYCD6;1* induction was largely abolished in *35S::ERF109-SRDX* compared with WT (Figures S6G and S6H). Together, these data indicate that ERF109 can directly induce promoter activity of *CYCD6;1*.

When we performed QC ablation and root tip resection experiments in *cycd6;1* and Col-0, the *cycd6;1* mutant exhibited similar stem cell niche regeneration capacity compared with WT, but a statistically significant impaired capacity of regeneration compared to WT when cut at and/or above zone II (Figures 6H-6L, S6I), while its meristem length was comparable with WT (Figure S6J). Collectively, our data indicate that CYCD6 is required for tissue regeneration (Figure 6M) and that combined input of JA and auxin signaling in regeneration is relevant in vascular and ground tissue cell types.

JA mediated wounding response and tissue regeneration accommodates soil penetration and parasitic pressure

As plant roots are at risk of physical damage during soil penetration, we explored the importance of a potential JA-mediated wounding response in soil penetration. When we transferred JA sensor *JAS9-VENUS* from 1/2 GM plates to a sand/soil mixture to grow for 4 days, the inverse JA signaling sensor *JAS9-VENUS* was reduced in WT but not in the *coi1-2* mutant under sand/soil conditions (Figures 7A, S7A, S7B), suggesting higher JA levels in plants grown in sand/soil conditions compared with growth on plate. To exclude that JAS9-VENUS is sensitive to touch response upon extraction from sand/soil, we also transferred seedlings from 1/2 GM plate to sand/soil, and immediately visualized JAS9-VENUS fluorescence levels were comparable (Figure S7C). We also observed induction of *ERF109*, *ERF115* and *CYCD6;1* promoter activity in sand/soil grown seedlings compared to seedlings kept on plate (Figure 7B), indicating that components of a JA-mediated response required for tissue regeneration are activated in roots during soil penetration. Consistently, in sand/soil, primary root growth of *cycd6;1*, *erf109* and *erf115*, *ERF115-SRDX* and *coi1-2* mutants was compromised compared to that of WT Col-0, whereas on plates primary root growth was comparable to Col-0 (Figure 7C). In summary, a JA-mediated regeneration response pathway is important for roots to penetrate soil.

JA plays an important role in defense response against insect herbivores, but whether this involves tissue repair and regeneration has not been clarified. To explore a role of JA-mediated wounding response and regeneration in nematode infection, we examined the spatiotemporal expression of key markers after root-knot nematode *Meloidogyne incognita* (*M. incognita*) infections. This 'stealth' nematode enters root tips and establishes a stable feeding site nearby (Jones et al., 2013). In a time course analysis of the expression of *JAS9-VENUS* during *M. incognita* infection, a significant decrease occurred at very early stage of *M. incognita* infection (Figures 7D, S7D-S7G). During feeding site initiation and gall formation, the fluorescence ratio of VENUS/RFP recovered but was still lower compared to that of non-infected control, indicating that root JA signaling level increases at early penetration stage and then reduces to intermediate levels (Figures 7D, S7D-S7G).

During *M. incognita* infection, we observed induction of both *ERF109* and *ERF115* promoters, and ectopic induction of *CYCD6;1* near sites of *M. incognita* infection, indicated by GUS staining (Figures 7E-7G, S7H-S7J). Time course experiments revealed that, during *M. incognita* infection*, ERF109* was induced during nematode penetration. *ERF115* and *CYCD6;1* were strongly induced in vascular and/or endodermal cells at all stages from penetration and feeding site initiation until gall formation (Figures S7H-S7J). These data, together with the expression pattern of JAS-VENUS, indicate that *M. incognita* infection activates a JA-mediated regeneration pathway in roots.

We compared primary root growth between Col-0 and *ERF115-SRDX* in the first few days after *M. incognita* invasion and feeding site initiation. Root growth in Col-0 in nematode-infected roots was reduced 52.4% compared with non-infected roots, whereas 78.3% reduction occurred in *ERF115-SRDX* (Figure 7H), suggesting impaired recovery of root growth after infection in *ERF115-SRDX*. To address whether defects in regeneration might affect susceptibility to nematode infections we counted numbers of egg masses at 7 weeks post inoculation. We found fewer egg masses in *ERF115-SRDX* and *coi1-2* compared with Col-0, and fewer egg masses per root tip in *ERF115-SRDX* and *erf109* compared with Col-0 (Figures 7I and S7K). These data suggest that JA-induced regeneration pathway promotes root growth after nematode invasion, and also promotes reproductive success of *M. incognita*.

CYCD6;1 was similary expressed in WT and *ERF115-SRDX* backgrounds without infection (Figure S7L), but after nematode infection induction of *CYCD6;1* in *ERF115-SRDX* background was delayed compared with WT (Figure 7J). Gall formation progressed slower in *ERF115-SRDX*, compared with WT at the same stage after infection (Figures 7J and 7K). EdU

(5-ethynyl-2'-deoxyuridine) incorporation assays revealed active DNA synthesis at the feeding sites of infected Col-0 roots, whereas less activity was detected at feeding sites of infected *ERF115-SRDX* roots (Figures 7L and 7M). For comparison, EdU incorporation in uninfected root meristems of Col-0 and *ERF115-SRDX* lines was comparable (Figures 7L and 7M). Together, these results confirm that *M. incognita* benefits from ERF109-ERF115 pathway activity.

Discussion

Plant development under normal growth conditions requires signaling pathways and transcription factor networks that steer the activity of meristems and their constituent stem cell niches. In addition, impressive accounts of plant developmental plasticity and regeneration from meristematic tissue have been described but the dramatic changes in gene expression in these studies have hitherto not been connected to the meristematic growth regulatory network (Efroni et al., 2016; Sena et al., 2009). We identify a core regeneration network that implicates a stress hormone jasmonate (JA)-mediated response in wounding induced regeneration of Arabidopsis roots (Figure 7N). JA-induced ERF109 is globally activated, stimulates *CYCD6;1* expression, functions upstream of ERF115 and promotes regeneration. ERF115 and CYCD6;1 are activated in stele and ground tissue respectively, and influence RBR and SCR activity by different mechanisms. Noteworthy, also auxin activates key regeneration regulators of this pathway. Soil penetration by roots and nematode herbivory of root systems, examples of abiotic and biotic stress conditions, induce this regeneration pathway to support growth.

Wounding has been considered as an early trigger of plant regeneration (Chen et al., 2016). JA accumulates within seconds to minutes after wounding (Figure S5) (Glauser et al., 2009; Larrieu et al., 2015), making it one of the candidates for the earliest wound signal. We reveal a synergy between auxin and JA in activating the ERF115 transcription factor involved in regeneration. This synergy may be relevant to simultaneously detect the two processes that occur upon wounding in tissue context: cell damage leading to JA accumulation, and tissue integrity loss leading to local auxin accumulation by impeded polar auxin transport (Figure 7N).

Some early signaling events triggering specific cellular responses and defense gene activation after wounding bear similarities between plants and animals (Mueller, 1998; Navarro et al., 2008). The cyclopentanoic fatty acid derivatives including the plant defense hormone JA is structurally similar to the animal defense regulators of the prostaglandin family (Creelman and Mullet, 1997; Yan et al., 2018). Both JA and prostaglandin are synthesized quickly in response to localized and/or systemic stress and inflammatory responses in plant or animal cells, respectively (Mueller, 1998). Interestingly, recent studies in animals reveal that prostaglandin PGE2 supports stem cell proliferation and survival, and inhibition of the prostaglandin-degrading enzyme potentiates tissue regeneration (Goessling et al., 2009; North et al., 2007;

Zhang et al., 2015b). Future studies should resolve whether JA and prostaglandin signaling derive from a common stress response pathway that predated plant and animal divergence.

Our studies reveal a critical role of JA in growth recovery during soil penetration and after *M. incognita* infections in Arabidopsis roots. JA signaling is activated both during soil penetration and early stages of nematode infection, and the JA dependent regeneration network is important for plants to adapt to parasitic pressure. Our ability to monitor a regeneration response after wounding and biotic insult using reporters that connect JA to developmental regulators paves the way to dissect biochemical defenses, trade-offs between defense and global plant growth, and body repair mechanisms. This should allow us to eventually comprehend how plants successfully cope with their environment.

Author Contributions

Conceptualization, W.Z. and B.S.; Methodology, W.Z. and B.S.; Investigation, W.Z., J.L., I.B., X.Z. and Q.Z.; Wring-Original Draft, W.Z. and B.S.; Writing-Review & Editing, W.Z., J.L., I.B., X.Z., G.S., C.L. and B.S.; Funding Acquisition, W.Z., C.L. and B.S.; Supervision, G.S., C.L. and B.S.

Declaration of Interests

The authors declare no competing interests.

Acknowledgements

We thank Lieven de Veylder, Cheng-Bin Xiang, Lin Xu, Philip Benfey, Laurent Laplaze, James A.H. Murray, Roberto Solano and the Nottingham Arabidopsis Stock Centre for sharing research materials. We thank Casper van Schaik and Axel Kuil for experimental help. We greatly appreciated helpful discussions with Jaap Bakker, Jian Xu, Niko Geldner and all members from the Scheres lab. This work was supported by an EMBO long-term fellowship (ALTF 784-2014 to W.Z.), the National Basic Research Program of China (Grant No. 2015CB942900 to C.L. W.Z. was further supported by this grant.) and the National Natural Science Foundation of China (Grant No. 31320103910 to C.L.).

References

Asahina, M., Azuma, K., Pitaksaringkarn, W., Yamazaki, T., Mitsuda, N., Ohme-Takagi, M., Yamaguchi, S., Kamiya, Y., Okada, K., Nishimura, T., *et al.* (2011). Spatially selective

hormonal control of RAP2.6L and ANAC071 transcription factors involved in tissue reunion in Arabidopsis. Proc. Natl. Acad. Sci. USA *108*, 16128-16132.
Blilou, I., Xu, J., Wildwater, M., Willemsen, V., Paponov, I., Friml, J., Heidstra, R., Aida, M., Palme, K., and Scheres, B. (2005). The PIN auxin efflux facilitator network controls growth and patterning in Arabidopsis roots. Nature *433*, 39–44.
Boter, M., Ruíz-Rivero, O., Abdeen, A., and Prat, S. (2004). Conserved MYC transcription factors play a key role in jasmonate signaling both in tomato and Arabidopsis. Genes Dev. *18*, 1577-1591.
Cai, X., Xu, P., Zhao, P., Liu, R., Yu, L., and Xiang, C. (2014). Arabidopsis ERF109 mediates cross-talk between jasmonic acid and auxin biosynthesis during lateral root formation. Nat. Commun. *5*, 5833.
Campos, M.L., Yoshida, Y., Major, I.T., De Oliveira Ferreira, D., Weraduwage, S.M., Froehlich, J.E., Johnson, B.F., Kramer, D.M., Jander, G., Sharkey, T.D., et al. (2016). Rewiring of jasmonate and phytochrome B signalling uncouples plant growth-defense tradeoffs. Nat. Commun. *7*, 12570.
Chen, L., Sun, B., Xu, L., and Liu, W. (2016). Wound signaling: The missing link in plant regeneration. Plant Signal. Behav. *11*, e1238548.
Chen, M., Chory, J., and Fankhauser, C. (2004). Light signal transduction in higher plants. Annu. Rev. Genet. *38*, 87–117.
Chen, Q., Sun, J., Zhai, Q., Zhou, W., Qi, L., Xu, L., Wang, B., Chen, R., Jiang, H., Qi, J., *et al.* (2011). The Basic Helix-Loop-Helix transcription factor MYC2 directly represses PLETHORA expression during jasmonate-mediated modulation of the root stem cell niche in Arabidopsis. Plant Cell *23*, 3335-3352.
Chen, R., Jiang, H., Li, L., Zhai, Q., Qi, L., Zhou, W., Liu, X., Li, H., Zheng, W., Sun, J., et al. (2012). The Arabidopsis mediator subunit MED25 differentially regulates jasmonate and abscisic acid signaling through interacting with the MYC2 and ABI5 transcription factors. Plant Cell. *24*, 2898-2918.
Creelman, R.A., and Mullet, J.E. (1997). Biosynthesis and action of jasmonates in plants. Annu. Rev. Plant Physiol. Plant Mol. Biol. *48*, 355-381.
Cruz-Ramirez, A., Diaz-Trivino, S., Blilou, I., Grieneisen, V.A., Sozzani, R., Zamioudis, C., Miskolczi, P., Nieuwland, J., Benjamins, R., Dhonukshe, P., *et al.* (2012). A bistable circuit involving SCARECROW-RETINOBLASTOMA integrates cues to inform asymmetric stem cell division. Cell *150*, 1002-1015.
Cruz-Ramirez, A., Diaz-Trivino, S., Wachsman, G., Du, Y., Arteaga-Vazquez, M., Zhang, H., Benjamins, R., Blilou, I., Neef, A.B., Chandler, V., *et al.* (2013). A SCARECROW-RETINOBLASTOMA protein network controls protective quiescence in the Arabidopsis root stem cell organizer. PLoS Biol. *11*, e1001724.
Dick, F.A. (2007). Structure-function analysis of the retinoblastoma tumor suppressor protein - is the whole a sum of its parts? Cell Div. *2*, 26.
Dombrecht, B., Xue, G.P., Sprague, S.J., Kirkegaard, J.A., Ross, J.J., Reid, J.B., Fitt, G.P., Sewelam, N., Schenk, P.M., Manners, J.M., *et al.* (2007). MYC2 differentially modulates diverse jasmonate-dependent functions in Arabidopsis. Plant Cell *19*, 2225-2245.
Efroni, I., Mello, A., Nawy, T., Ip, P.L., Rahni, R., Delrose, N., Powers, A., Satija, R., and Birnbaum, K.D. (2016). Root Regeneration Triggers an Embryo-like Sequence Guided by Hormonal Interactions. Cell *165*, 1721–1733.
Fernández-Calvo, P., Chini, A., Fernández-Barbero, G., Chico, J.-M., Gimenez-Ibanez, S., Geerinck, J., Eeckhout, D., Schweizer, F., Godoy, M., Franco-Zorrilla, J.M., et al. (2011). The *Arabidopsis* bHLH Transcription Factors MYC3 and MYC4 Are Targets of JAZ Repressors and Act Additively with MYC2 in the Activation of Jasmonate Responses. Plant Cell. *23*, 701-715.

Gehl, C., Waadt, R., Kudla, J., Mendel, R.R., and Hänsch, R. (2009). New GATEWAY vectors for high throughput analyses of protein-protein interactions by bimolecular fluorescence complementation. Mol. Plant *2*, 1051–1058.
Glauser, G., Dubugnon, L., Mousavi, S.A., Rudaz, S., Wolfender, J.L., and Farmer, E.E. (2009). Velocity estimates for signal propagation leading to systemic jasmonic acid accumulation in wounded Arabidopsis. J. Biol. Chem. *284*, 34506-34513.
Glauser, G., Grata, E., Dubugnon, L., Rudaz, S., Farmer, E.E., and Wolfender, J.L. (2008). Spatial and temporal dynamics of jasmonate synthesis and accumulation in Arabidopsis in response to wounding. J. Biol. Chem. *283*, 16400-16407.
Goessling, W., North, T.E., Loewer, S., Lord, A.M., Lee, S., Stoick-Cooper, C.L., Weidinger, G., Puder, M., Daley, G.Q., Moon, R.T., et al. (2009). Genetic interaction of PGE2 and Wnt signaling regulates developmental specification of stem cells and regeneration. Cell *136*, 1136-1147.
Heyman, J., Canher, B., Bisht, A., Christiaens, F., and De Veylder, L. (2017). Emerging role of the plant ERF transcription factors in coordinating wound defense responses and repair. J. Cell Sci. *131*, jcs208215.
Heyman, J., Cools, T., Canher, B., Shavialenka, S., Traas, J., Vercauteren, I., Van den Daele, H., Persiau, G., De Jaeger, G., Sugimoto, K., *et al.* (2016). The heterodimeric transcription factor complex ERF115-PAT1 grants regeneration competence. Nat. Plants *2*, 16165.
Heyman, J., Cools, T., Vandenbussche, F., Heyndrickx, K.S., Van Leene, J., Vercauteren, I., Vanderauwera, S., Vandepoele, K., De Jaeger, G., Van Der Straeten, D., *et al.* (2013). ERF115 controls root quiescent center cell division and stem cell replenishment. Science *342*, 860-863.
Hickman, R., Van Verk, M.C., Van Dijken, A.J.H., Mendes, M.P., Vroegop-Vos, I.A., Caarls, L., Steenbergen, M., Van der Nagel, I., Wesselink, G.J., Jironkin, A., *et al.* (2017). Architecture and Dynamics of the Jasmonic Acid Gene Regulatory Network. Plant Cell *29*, 2086-2105.
Hou, X., Lee, L.Y.C., Xia, K., Yen, Y., and Yu, H. (2010). DELLAs modulate jasmonate signaling via competitive binding to JAZs. Dev. Cell *19*, 884-894.
Ikeuchi, M., Iwase, A., Rymen, B., Lambolez, A., Kojima, M., Takebayashi, Y., Heyman, J., Watanabe, S., Seo, M., De Veylder, L., et al. (2017). Wounding triggers callus formation via dynamic hormonal and transcriptional changes. Plant Physiol. *175*, 1158-1174.
Ikeuchi, M., Shibata, M., Rymen, B., Iwase, A., Bgman, A.M., Watt, L., Coleman, D., Favero, D.S., Takahashi, T., Ahnert, S.E., et al. (2018). A Gene Regulatory Network for Cellular Reprogramming in Plant Regeneration. Plant Cell Physiol. *59*, 770-782.
Jones, J.T., Haegeman, A., Danchin, E.G.J., Gaur, H.S., Helder, J., Jones, M.G.K., Kikuchi, T., Manzanilla-López, R., Palomares-Rius, J.E., Wesemael, W.M.L., et al. (2013). Top 10 plant-parasitic nematodes in molecular plant pathology. Mol. Plant Pathol. *14*, 946–961.
Karasov, T.L., Chae, E., Herman, J.J., and Bergelson, J. (2017). Mechanisms to Mitigate the Trade-Off between Growth and Defense. Plant Cell. *29*, 666-680.
Kareem, A., Durgaprasad, K., Sugimoto, K., Du, Y., Pulianmackal, A.J., Trivedi, Z.B., Abhayadev, P. V, Pinon, V., Meyerowitz, E.M., Scheres, B., et al. (2015). PLETHORA genes control regeneration by a two-step mechanism. Curr. Biol. *25*, 1017–1030.
Kehn, K., De La Fuente, C., Strouss, K., Berro, R., Jiang, H., Brady, J., Mahieux, R., Pumfery, A., Bottazzi, M.E., and Kashanchi, F. (2005). The HTLV-I Tax oncoprotein targets the retinoblastoma protein for proteasomal degradation. Oncogene. *24*, 525-540.
Kong, X., Tian, H., Yu, Q., Zhang, F., Wang, R., Gao, S., Xu, W., Liu, J., Shani, E., Fu, C., et al. (2018). PHB3 Maintains Root Stem Cell Niche Identity through ROS-Responsive AP2/ERF Transcription Factors in Arabidopsis. Cell Rep. *22*, 1350-1363.

Koornneef, A., and Pieterse, C.M. (2008). Cross talk in defense signaling. Plant Physiol. *146*, 839-844.
Kuchen, E.E., Fox, S., De Reuille, P.B., Kennaway, R., Bensmihen, S., Avondo, J., Calder, G.M., Southam, P., Bangham, A., and Coen, E. (2012). Generation of leaf shape through early patterns of growth and tissue polarity. Science *335*, 1092-1096.
Larrieu, A., Champion, A., Legrand, J., Lavenus, J., Mast, D., Brunoud, G., Oh, J., Guyomarc'h, S., Pizot, M., Farmer, E.E., *et al.* (2015). A fluorescent hormone biosensor reveals the dynamics of jasmonate signalling in plants. Nat. Commun. *6*, 6043.
Li, H., Torres-Garcia, J., latrasse, D., Benhamed, M., Schilderink, S., Zhou, W., Kulikova, O., Hirt, H., and Bisseling, T. (2017). Plant-specific histone deacetylases HDT½ regulate GIBBERELLIN 2-OXIDASE 2 expression to control Arabidopsis root meristem cell number. Plant Cell *29*, 2183-2196.
Melnyk, C.W., Gabel, A., Hardcastle, T.J., Robinson, S., Miyashima, S., Grosse, I., and Meyerowitz, E.M. (2018). Transcriptome dynamics at *Arabidopsis* graft junctions reveal an intertissue recognition mechanism that activates vascular regeneration. Proc. Natl. Acad. Sci. *115*, E2447-E2456
Mueller, M.J. (1998). Radically novel prostaglandins in animals and plants: the isoprostanes. Chem. Biol. *5*, R323-333.
Nakagawa, T., Kurose, T., Hino, T., Tanaka, K., Kawamukai, M., Niwa, Y., Toyooka, K., Matsuoka, K., Jinbo, T., and Kimura, T. (2007). Development of series of gateway binary vectors, pGWBs, for realizing efficient construction of fusion genes for plant transformation. J. Biosci. Bioeng. *104*, 34–41.
Navarro, L., Bari, R., Achard, P., Lison, P., Nemri, A., Harberd, N.P., and Jones, J.D.G. (2008). DELLAs control plant immune responses by modulating the balance of jasmonic acid and salicylic acid signaling. Curr. Biol. *18*, 650-655.
Nemhauser, J.L., Hong, F.X., and Chory, J. (2006). Different plant hormones regulate similar processes through largely nonoverlapping transcriptional responses. Cell *126*, 467–475.
North, T.E., Goessling, W., Walkley, C.R., Lengerke, C., Kopani, K.R., Lord, A.M., Weber, G.J., Bowman, T. V., Jang, I.H., Grosser, T., et al. (2007). Prostaglandin E2 regulates vertebrate haematopoietic stem cell homeostasis. Nature *447*, 1007-1011.
Ortega-Martínez, O., Pernas, M., Carol, R.J., and Dolan, L. (2007). Ethylene modulates stem cell division in the Arabidopsis thaliana root. Science *317*, 507–510.
Pieterse, C.M.J., Van der Does, D., Zamioudis, C., Leon-Reyes, A., and Van Wees, S.C.M. (2012). Hormonal modulation of plant immunity. Annu. Rev. Cell Dev. Biol. *28*, 489-521.
Sena, G., Wang, X.N., Liu, H.Y., Hofhuis, H., and Birnbaum, K.D. (2009). Organ regeneration does not require a functional stem cell niche in plants. Nature *457*, 1150-1110.
Sheard, L.B., Tan, X., Mao, H., Withers, J., Ben-Nissan, G., Hinds, T.R., Kobayashi, Y., Hsu, F.F., Sharon, M., Browse, J., *et al.* (2010). Jasmonate perception by inositol-phosphate-potentiated COI1-JAZ co-receptor. Nature *468*, 400-405.
Shimotohno, A., Heidstra, R., Blilou, I., and Scheres, B. (2018). Root stem cell niche organizer specification by molecular convergence of PLETHORA and SCARECROW transcription factor modules. Genes Dev. doi:10.1101/gad.314096.118
Sozzani, R., Cui, H., Moreno-Risueno, M.A., Busch, W., Van Norman, J.M., Vernoux, T., Brady, S.M., Dewitte, W., Murray, J.A., and Benfey, P.N. (2010). Spatiotemporal regulation of cell-cycle genes by SHORTROOT links patterning and growth. Nature *466*, 128-132.
Sugimoto, K., Jiao, Y., and Meyerowitz, E.M. (2010). Arabidopsis regeneration from multiple tissues occurs via a root development pathway. Dev. Cell *18*, 463–471.
Sun, J., Xu, Y., Ye, S., Jiang, H., Chen, Q., Liu, F., Zhou, W., Chen, R., Li, X., Tietz, O., et al. (2009). Arabidopsis ASA1 Is Important for Jasmonate-Mediated Regulation of Auxin Biosynthesis and Transport during Lateral Root Formation. Plant Cell *21*, 1495-1511.

Wang, Z., Cao, G., Wang, X., Miao, J., Liu, X., Chen, Z., Qu, L.J., and Gu, H. (2008). Identification and characterization of COI1-dependent transcription factor genes involved in JA-mediated response to wounding in Arabidopsis plants. Plant Cell Rep. *27*, 125-135.
Warmerdam, S., Sterken, M.G., van Schaik, C., Oortwijn, M.E.P., Sukarta, O.C.A., Lozano-Torres, J.L., Dicke, M., Helder, J., Kammenga, J.E., Goverse, A., et al. (2018). Genome-wide association mapping of the architecture of susceptibility to the root-knot nematode Meloidogyne incognita in Arabidopsis thaliana. New Phytol. *218*, 724-737.
Vilarrasa-Blasi, J., González-García, M.P., Frigola, D., Fàbregas, N., Alexiou, K.G., López-Bigas, N., Rivas, S., Jauneau, A., Lohmann, J.U., Benfey, P.N., et al. (2014). Regulation of plant stem cell quiescence by a brassinosteroid signaling module. Dev. Cell *30*, 36–47.
Wasternack, C., and Hause, B. (2013). Jasmonates: biosynthesis, perception, signal transduction and action in plant stress response, growth and development. An update to the 2007 review in Annals of Botany. Ann. Bot. *111*, 1021-1058.
Xie, D.X., Feys, B.F., James, S., Nieto-Rostro, M., and Turner, J.G. (1998). COI1: an Arabidopsis gene required for jasmonate-regulated defense and fertility. Science *280*, 1091-1094.
Xu, L., Liu, F., Lechner, E., Genschik, P., Crosby, W., Ma, H., Peng, W., Huang, D., Xie, D. (2002). The SCFCOI1 Ubiquitin-Ligase Complexes Are Required for Jasmonate Response in Arabidopsis. Plant Cell *14*, 1919–1935.
Xu, J., Hofhuis, H., Heidstra, R., Sauer, M., Friml, J., and Scheres, B. (2006). A molecular framework for plant regeneration. Science *311*, 385-388.
Xu, L., and Huang, H. (2014). Genetic and epigenetic controls of plant regeneration. Curr. Top. Dev. Biol. *108*, 1-33.
Yang, D., Yao, J., Mei, C., Tong, X., Zeng, L., Li, Q., Xiao, L., Sun, T., Li, J., Deng, X., *et al.* (2012). Plant hormone jasmonate prioritizes defense over growth by interfering with gibberellin signaling cascade. Proc Natl Acad Sci USA *109*, E1192-E1200.
Yan, C., Fan, M., Yang, M., Zhao, J., Zhang, W., Su, Y., Xiao, L., Deng, H., and Xie, D. (2018). Injury Activates Ca2+/Calmodulin-dependent phosphorylation of JAV1-JAZ8-WRKY51 complex for jasmonate biosynthesis. Mol. Cell *70*, 136-149.
Yan, J., Zhang, C., Gu, M., Bai, Z., Zhang, W., Qi, T., Cheng, Z., Peng, W., Luo, H., Nan, F., et al. (2009). The Arabidopsis CORONATINE INSENSITIVE1 protein is a jasmonate receptor. Plant Cell *21*, 2220–2236.
Zhang, F., Yao, J., Ke, J., Zhang, L., Lam, V.Q., Xin, X.F., Zhou, X.E., Chen, J., Brunzelle, J., Griffin, P.R., et al. (2015a). Structural basis of JAZ repression of MYC transcription factors in jasmonate signalling. Nature *525*, 269–273.
Zhang, H., Han, W., De Smet, I., Talboys, P., Loya, R., Hassan, A., Rong, H., Jürgens, G., Paul Knox, J., and Wang, M.H. (2010). ABA promotes quiescence of the quiescent centre and suppresses stem cell differentiation in the Arabidopsis primary root meristem. Plant J. *64*, 764-774.
Zhang, X., Zhou, W., Chen, Q., Fang, M., Zheng, S., Scheres, B., and Li, C. (2018). Mediator subunit MED31 is required for radial patterning of Arabidopsis roots. Proc. Natl. Acad. Sci. *115*, E5624–E5633.
Zhang, Y., Desai, A., Yang, S.Y., Bae, K.B., Antczak, M.I., Fink, S.P., Tiwari, S., Willis, J.E., Williams, N.S., Dawson, D.M., et al. (2015b). Inhibition of the prostaglandin-degrading enzyme 15-PGDH potentiates tissue regeneration. Science *348*, aaa2340.

Figure legends

Figure 1. JA acts through RBR-SCR to regulate QC quiescence.

(A-I) Modified pseudo-Schiff propidium iodide (mPS-PI) staining in stem cell niche of WT Col-0 (A-C), *pWOX5::amiGORBR* (Reducing RBR specifically in QC (quiescent center)) (D-F), and *pSCR::SCRaca-YFP* (RBR-interaction defective allele) (G-I). Scale bar, 25 μm.

(J-L) QC cell number of indicated genotypes without or with (hereafter +/-) MeJA treatment. n denotes total number of scored samples. Box plots display median (line), interquartile range (box), whiskers (extending 1.5 times the interquartile range), sample mean (cross) and outliers (dot). Lowercase letters indicate statistically different groups (Student's *t*- test, $P < 0.01$).

See also Figure S1.

Figure 2 JA induces *ERF115* transcription

(A-D) mPS-PI staining in *ERF115-OE* and *ERF115-SRDX* stem cell niches +/- MeJA treatment. Scale bar, 25 μm.

(E) QC cell number quantification of indicated genotypes +/- MeJA treatment. Data represent mean ± SD (standard deviation) of 2 independent experiments with >10 replicates per treatment in each genotype.

(F-K) MeJA induction of *ERF115* in QC and vascular cells. Arrows mark QC cells with GFP signal or GUS stain only after MeJA treatment. Scale bars, 50 μm.

(L) Quantification of *pERF115:GUS-GFP* positive QC cells +/- MeJA treatment. Data represent mean ± SD of 3 independent experiments.

(M) RT-qPCR reveals that MeJA induction of *ERF115* depends on COI1 and partially on MYC2. *ERF115* transcript level in Col-0 without JA treatment was arbitrarily set to 1. Data represent mean ± SEM (standard error) of 3 independent experiments. Different lowercase letters indicate statistically different groups (Tukey's test, $P < 0.05$).

(N and O) (N) Diagram of DNA fragments (No.1-8) in *ERF115* promoter used for ChIP-qPCR. (O) ChIP-qPCR of MYC2 on the promoter of *ERF115*. Peak fragment (No. 3) contains a typical MYC2-binding G-box (CACGTG) motif. ChIP signal was quantified as percentage of total input DNA by qPCR, and normalized to Col-0 fragment 1(set as 1). Data represent mean ± SEM of 3 independent experiments. IR, intergenic region. (Student's *t*- test, $^*P < 0.05$, $^{**}P < 0.01$)

(P) Diagram of *ERF115* and *mERF115* promoter structures.

(Q) Representative images of GUS staining of *pERF115::GUS* and *pmERF115::GUS* +/- MeJA treatment for 6 hours. Nine independent *pERF115::GUS* and nine *pmERF115::GUS* lines were analysed separately with consistent results. Scale bars, 100 µm.
See also Figure S2.

Figure 3 **Genetic interaction between RBR-SCR and ERF115**
(A-J) Representative confocal images of indicated genotypes at 6 DAG. Scale bar, 50 µm.
(K) Box plots of QC cell number in the indicated lines, n denotes total number of scored samples. Box plots display median (line), interquartile range (box), whiskers (extending 1.5 times the interquartile range), sample mean (cross) and outliers (dot). Lowercase letters indicate statistically different groups (Student's *t*- test, $P < 0.05$, $^{**}P < 0.01$).
(L) Schematic diagram of JA-mediated molecular network which activates the root stem cell niche. Arrows represent activation; bar-headed lines represent repression; lines represent interactions between RBR and ERF115, and RBR and SCR, respectively.
See also Figure S3.

Figure 4 **JA signaling promotes stem cell niche regeneration**
(A-F) Time course after columella stem cell (CSC) laser ablation of *pWOX5::GFP* +/- MeJA treatment. Same root: A-C; Same root: D-F. Blue arrows mark ablated CSCs.
(G) Quantification of new columella cell layers between QC (marked by *pWOX5::GFP*) and ablated CSCs during the time course. Data represent mean ± SEM of 3 independent experiments with at least 5 technical replicates per treatment.
(H-K) QC laser ablation in *pWOX5::GFP* and *coi1-1 pWOX5::GFP* genotypes.
(L and M) Quantification of new columella cell layers between QC and ablated cells after partial (L) or whole (M) QC ablation in indicated genotypes. Data represent mean ± SEM of 3 independent experiments with at least 6 technical replicates per genotype.
(N) Quantification of *JAS9-VENUS* JA biosensor fluorescence with or without QC ablation in WT and *coi1-2*. Fluorescence intensity without ablation or immediately after ablation (<30s) was set to 1 in WT and *coi1-2*, respectively. Error bars represent SE, n>9. TAA, time after ablation.
(O-T) QC laser ablation in *ERF115-OE pWOX5::GFP*, *pWOX5::GFP*, and *ERF115-SRDX*

pWOX5::GFP genotypes performed at 3 DAG.

(U) Quantification of new columella cell layers between QC and ablated cells after QC ablation in indicated genotypes. Data represent mean ± SEM of 3 independent experiments with at least 6 technical replicates per genotype.

(V) Schematic diagram of JA-mediated molecular network which activates QC and regulates stem cell niche regeneration. SCN, stem cell niche.

For (H-K and O-T), White arrows mark stem cell niche regeneration, blue arrows mark ablated QC cells. White brackets indicate columella layers between new QC and ablated cells.

Scale bars, 50 µm. See also Figure S4.

Figure 5 **ERF109 responds quickly to JA and wounding, and is required for tissue regeneration**

(A and B) Root tip regeneration of *35S::amiGORBR pRBR::RBR-YFP* and *35S::amiGORBR* after resection. Images display same category III resected root with regenerated tip in *35S::amiGORBR* (B) and same resected root with differentiated root tip in *35S::amiGORBR pRBR::RBR-YFP* (A).

(C) Quantification of the frequency of regeneration and meristem length in indicated genotypes 72 hours after resection. Root tip resection categories based on cut site distance from tip: I, cut site at QC; II, half of the meristem cut; III, 3/4 of the meristem cut; IV, whole meristem cut. Error bars represent SD from two independent experiments with at least 30 technical replicates per genotype. Meristem length was measured at 3 DAG. Error bars represent SD (n=12). Same lowercase letters indicate absence of statistical difference (Student's *t*- test, *$P < 0.05$).

(D) Representative confocal images of *pERF109::GFP* genotype +/- 50 µM MeJA treatment for 2 hours.

(E) RT-qPCR reveals that MeJA induces *ERF109*. *ERF109* transcript level in Col-0 without JA treatment was arbitrarily set to 1. Data represent mean ± SEM of 3 independent experiments. Lowercase letters indicate statistically different groups (Tukey's test, $P < 0.05$).

(F) ChIP-qPCR of MYC2 on the promoter of *ERF109*. The ChIP signal was quantified as the percentage of total input DNA by qPCR, and normalized to the signal of *MYC2-GFP* IR fragment (set as 1). Data represent mean ± SEM of 3 independent experiments. IR, intergenic region. (Student's *t*- test, *P < 0.05).

(G) GUS staining of *pERF109::GUS* 30 min after root-tip resection.

(H) GUS staining of *pERF109::GUS* and *coi1-1 pERF109::GUS* genotypes at 3 hours after resection.

(I and J) RT-qPCR of *ERF115* and *ERF109* in indicated genotypes. *ERF115* and *ERF109* transcript level in Col-0 respectively, was set to 1. Data represent mean ± SEM of 3 independent experiments. Different lowercase letters indicate statistically different groups (Tukey's test, P < 0.01).

(K and L) Root tip regeneration of *pWOX5::GFP* and *pWOX5::GFP erf109* genotypes after resection. Images display regenerated root tip in WT (K) and differentiated root tip in *erf109* (L) at category III.

(M) Quantification of the frequency of regeneration in *pWOX5::GFP* and *pWOX5::GFP erf109,* 72 hours after resection. Data represent mean ± SD of 3 independent experiments with at least 30 technical replicates per genotype. Student's *t*- test, *P < 0.05, **P < 0.01.

(N) Quantification of the frequency of regeneration in *pWOX5::GFP* and *pWOX5::GFP coi1-1*. Data represent mean ± SD of 3 independent experiments. Student's *t*- test, *P < 0.05.

(O) Schematic diagram of JA-mediated molecular network which activates QC, regulates stem cell niche and tissue regeneration.

Scale bars, 50 µm. See also Figure S5.

Figure 6 **Synergy between JA and auxin signaling in regulating regeneration.**

(A-D) GUS staining of *pERF115:GUS-GFP* with mock or indicated treatments for 4 hours, respectively.

(E) RT-qPCR analysis of *ERF115* transcripts with mock or indicated treatments for 4 hours, respectively. Data represent mean ± SEM of 3 independent experiments. Lowercase letters distinguish statistically different groups (Tukey's test, P < 0.05).

(F) Expression of *pCYCD6;1::GUS-GFP* +/- MeJA treatment. 6 DAG seedlings were treated +/- 50 µM MeJA for 3h before imaging. n>10.

(G) Dual-luciferase assays. Expression of *pCYCD6;1::LUC* reporter only was set to 1. fLUC, Firefly luciferase; rLUC, Renilla luciferase. Transfection efficiency was normalized with a constitutively expressed rLUC. Data represent mean ± SD of 3 independent experiments. Student's *t*- test, ***P < 0.001.

(H) Frequency of regeneration in Col-0 and *cycd6;1*. Data represent mean ± SD of 3 independent experiments with at least 30 technical replicates per genotype. Student's *t*- test, $*P < 0.05$.

(I-L) Root tip regeneration of Col-0 and *cycd6;1* after resection. Pictures shown are single root regeneration (Same root: I and J; Same root: K and L. Cut site: category III, regenerated root tip in Col-0 (J) and differentiated root tip in *cycd6;1* (L)).

(M) Schematic diagram of JA and auxin-mediated molecular network which activates QC, regulates stem cell niche and tissue regeneration.

Scale bars, 50 µm.

Figure 7 **JA mediated wounding response and tissue regeneration is important to accommodate soil penetration and parasitic pressure**

(A) Expression of *JAS9-VENUS* and *JAS9-VENUS coi1-2* in roots grown on plate or in sand. Scale bar, 100 µm.

(B) Expression of the indicated genotypes on plate or in sand. Scale bars, 1 cm for plates, and 100 µm for confocal images. n>12.

(C) Primary root length of the indicated genotypes growing on plate or in sand. Data represent mean ± SEM of 3 independent experiments with at least 16 technical replicates per genotype. Student's *t*- test, $*P < 0.05$, $***P < 0.001$.

(D) Fluorescence ratio of *JAS9-VENUS*/*H2B-RFP* at different stages of nematode (*Meloidogyne incognita*) infections. Bars represent SE. n denotes the total number of samples scored. Lowercase letters indicate statistically different groups. Student's *t*- test, $P < 0.01$.

(E-G) GUS staining of *pERF109::GUS* (E), *pERF115::GUS-GFP* (F) and *pCYCD6;1::GUS-GFP* (G) +/- nematode infections. DPI, days post infection.

(H) Recovery of primary root growth +/- nematode infection in Col-0 and *ERF115-SRDX*. Root lengths represent primary root growth from 2 dpi to 6 dpi for mock, or root growth from galls (2 dpi) to root tips (6 dpi) for infected roots. n denotes the total number of samples scored from two independent experiments. Box plots display median (line), interquartile range (box), whiskers (extending 1.5 times the interquartile range), sample mean (cross) and outliers (dot). Student's *t*- test, $***\ P < 0.001$.

(I) Average area of galls per plant in the indicated genotypes at 7 weeks post infection. Data represent mean ± SEM of 3 independent experiments with 6 replicates per genotype. Lowercase letters indicate statistically different groups. Student's *t*- test, $P < 0.05$.

(J and K) GUS staining of *pCYCD6;1::GUS-GFP* and *pCYCD6;1::GUS-GFP ERF115-SRDX* at 2 or 3 dpi.

(L and M) EdU incorporation assays in uninfected and infected roots of Col-0 and *ERF115-SRDX*. EdU incorporations show active DNA synthesis (S-phase) at feeding sites of infected Col-0 roots, whereas few EdU positive nuclei at feeding sites of infected *ERF115-SRDX* roots. Dashed white lines: nematodes.

(N) Schematic diagram of JA and auxin-mediated molecular network which activates the root stem cell niche and promote stem cell niche and tissue regeneration after damage. Arrows represent activations; bar-headed arrows represent repressions; lines represent interactions between RBR and ERF115, RBR and SCR, and SCR and SHR, respectively.

(E-M) Scale bars, 50 µm. See also Figure S7.

Supplemental figure 1 **JA induces QC division through the SHR-SCR-RBR network. Related to Figure 1.**

(A) Median longitudinal view of *Arabidopsis* root stem cell niche organization. Red, QC; Green, initials surrounding QC. Red line outlines the root stem cell niche.

(B-C) EdU incorporation assays showing that JA promotes QC division. 3 DAG Col-0 seedlings were grown on 1/2 GM +/- MeJA treatment for 44 hours, and then cultured with EdU for 2 hours before EdU incorporation in the root stem cell niche was examined. Arrows highlight EdU stain in nuclei of QC after MeJA treatment, but not in nuclei of QC from seedlings grown on 1/2 GM. Scale bar, 25 µm.

(D-M) Genetic interaction between COI1 and SCR-RBR. Indicated genotypes were grown on 1/2 GM +/- MeJA 50 µM for 48 hours. Data shown are mean ± SD, n>10. Same lowercase letters indicate no statistically different between groups (Student's *t*- test, $P < 0.05$). Scale bars, 50 µm.

(N-T) Representative confocal images of indicated lines +/- MeJA 50 µM treatment for 48 hours. MeJA promotes QC division in Col-0 but not in *scr-3* and *shr-2* mutants. Data shown are mean ± SD, n>15. Different lowercase letters indicate significant differences between groups (Student's *t*- test, $P < 0.01$). Scale bars, 50 µm.

(U-Z) Confocal images of *pSCR::GFP* (U and V), *pSCR::SCR-YFP* (W and X) and *pRBR::RBR-YFP* (Y and Z) +/- 50 µM MeJA for 24 hours. Scale bars, (W and X) 25 µm, (U and V) and (Y and Z) 50 µm.

(AA) RT-qPCR analysis of *SCR* and *RBR* transcripts +/- MeJA treatment for 24 hours. Data represent mean ± SEM of 3 independent experiments.

Supplemental figure 2 **JA, BR and ROS-mediated transcriptional regulation of *ERF115*. Related to Figure 2.**

(A) QC cell number in Col-0 and *erf115* +/- MeJA 50 µM treatment for 48 hours.

(B) Representative images of GUS staining of *pERF115::GUS-GFP* +/- MeJA treatment for 1 hour or 3 hours. After MeJA treatment for 1 hour, weak GUS stain can be found at vascular cells (arrow). Scale bar, 50 µm.

(C) Hand section of root tips of *pERF115::GUS-GFP* +/- MeJA treatment reveals protoxylem fluorescence. Samples were fixed in 4% paraformaldehyde and stained with SCRI Renaissance 2200. Scale bar, 20 µm.

(D) QC cell number in Col-0 and *coi1-2* +/- 24-epiBL (brassinolide) 500 nM or 24-epiBL+MeJA 50 µM treatment for 48 hours.

(E) Representative confocal images of indicated lines +/- 1 µM 24-epiBL treatment for 20 hours. Scale bar, 50 µm.

(F) QC cell number in Col-0 and *coi1-2* +/- H_2O_2 200 µM or H_2O_2 200 µM+MeJA 20 µM treatments for 48 hours.

(G) Representative images of GUS staining of indicated lines +/- 1 mM H_2O_2 treatment for 16 hours. Scale bar, 50 µm.

Data are mean ± SD. n denotes total number of samples scored. Different lowercase letters indicate significant differences between groups (Tukey's test, $P < 0.05$).

Supplemental figure 3 **RBR interacts with ERF115. Related to Figure 3,** (A-E) Representative confocal images of the indicated genotypes at 5 DAG. Scale bar, 50 µm.

(F) Schematic diagram of the ERF115 protein. AP2, AP2 DNA-binding domain; LxFxE, Leu-x-Phe-x-Glu motif; pink boxes, low complexity regions. Software, SMART.

(G) Yeast two hybrid assays showing that RBR interacts with ERF115. Yeast transformants were dropped onto SD/-Trp/-Leu (-LW), SD/-His/-Trp/-Leu (-HLW) and SD/-Ala/-His/-Trp/-Leu (-AHLW) media to assess protein–protein interactions. ERF115m, ERF115 protein with mutated LxFxE motif (AxAxA). SCR-SHR and RBR-SCR interactions were used as positive controls. Negative controls: empty BD+ERF115-AD; RBR-BD+empty AD. AD, GAL4 activation domain; BD, binding domain.

(H) Bimolecular fluorescence complementation assays showing that RBR interacts with ERF115 in planta. Indicated different combinations were co-infiltrated into *N. benthamiana* leaves. Positive controls: SCR-nYFP+SHR-cYFP; RBR-nYFP+SCR-cYFP. Negative controls: RBR-nYFP+RBR-cYFP; ERF115-nYFP+ERF115-cYFP; RBR-nYFP+empty cYFP; ERF115-nYFP+cYFP-ERF115; ERF115-nYFP+cYFP-ERF115-SRDX. ERF115m, ERF115 protein with mutated LxFxE motif; nYFP, N-terminal fragment of VENUS YFP; cYFP, C-terminal fragment of VENUS YFP. Scale bar, 50 µm.

(I) Co-IP assays of RBR with ERF115 (SRDX). *35S::RBR-myc* and *35S::GFP-ERF115 (SRDX)* were infiltrated into *N. benthamiana* leaves. Protein samples immunoprecipitated with anti-myc antibody and immunoblotted with anti-GFP antibody. *, mouse antibody heavy chain.

Supplemental figure 4 **JA signaling promotes stem cell niche regeneration. Related to Figure 4.**

(A-B’’’) Time course of columella stem cell (CSC) laser ablation of *pWOX5::GFP* +/- MeJA pre-treatment. Images display the same root for A and B, repectively. Two-day-old seedlings were transferred to plates +/- 50 µM MeJA for 24 hours before laser ablation was performed. Blue arrows mark ablated CSCs.

(C-D’) Time course of columella stem cell (CSC) laser ablation *of pWOX5::GFP* +/- MeJA treatment. Three-day-old seedlings were CSC ablated and then transferred to plates +/- 250 nM MeJA. Blue arrows mark ablated CSCs.

(E) Quantification of columella cell layers between QC (marked by *pWOX5::GFP*) and ablated CSCs during the time course. Data represent mean ± SEM of 3 independent experiments with at least 5 technical replicates per treatment.

(F-G''') Time course of QC laser ablation of *pWOX5::GFP* and *coi1-1 pWOX5::GFP* genotypes.

(H-I''') Time course of QC laser ablation of *JAS9-VENUS* JA biosensor in WT and *coi1-2*. White dashed circles indicate photobleached region by laser ablation (including ablated QC). Insets in H' and I' show ablated QC cells with PI-staining nuclei.

(J-K'') Time course of QC laser ablation of *pERF115::GUS-GFP* in WT and *coi1-2*.

(L) Quantification of fluorescence of *pERF115::GUS-GFP* in WT and *coi1-2* after QC ablation. Data represent mean ± SEM of 2 independent experiments with at least 6 technical replicates per genotype. Student's *t*- test, * $P < 0.05$.

(M-P''') Time course of QC laser ablation of *ERF115-OE pWOX5::GFP*, *pWOX5::GFP*, *ERF115-SRDX pWOX5::GFP* and *erf115 pWOX5::GFP* genotypes.

(Q-R') QC laser ablation of *pSCR::SCRwt-YFP pWOX5-GFP/scr-4* and *pSCR::SCRaca-YFP pWOX5-GFP/scr-4* genotypes. In *pSCR::SCRaca-YFP pWOX5-GFP/scr-4*, no *SCR* or *WOX5* was expressed in the newly regenerated "QC".

(S) Quantification of new columella cell layers between QC and ablated cells after QC ablation in the indicated genotypes. Data represent mean ± SEM of 3 independent experiments.

(T) Quantification of new columella cell layers between QC and ablated cells after QC ablation in the indicated genotypes. Data represent mean ± SEM of 3 independent experiments.

(U-V''') Time course of QC laser ablation of *pWOX5::amiGORBR* and *ERF115-SRDX pWOX5::GUS-GFP pWOX5::amigoRBR* genotypes.

(W-X''') Time course of QC laser ablation of *pSCR::SCRaca-YFP pCYCD6;1::GFP/scr-4* and *ERF115-SRDX pSCR::SCRaca-YFP pCYCD6;1::GFP/scr-4* genotypes.

(Y) Quantification of new columella cell layers between QC and ablated cells after QC ablation in the indicated genotypes. Data represent mean ± SEM of 3 independent experiments.

Scale bars, 50 µm. For (C-X), laser ablation was performed at 3 DAG. White arrows mark stem cell niche regeneration, blue arrows mark ablated QC cells.

Supplemental figure 5 ***ERF109* acts upstream of *ERF115* in response to wounding. Related to Figure 5.**

(A and B) Time-course confocal images of *JAS9-VENUS* and *JAS9-VENUS coi1-2* at indicated time points after root tip resection.

(C) Fluorescence ratio of *JAS9-VENUS* /*H2B-RFP* at different time points after root tip resection. Error bars represent SE, n>8.

(D and E) Time course of root tip resection of *pERF115::GUS-GFP* in WT and *coi1-2*.

(F) Quantification of fluorescence of *pERF115::GUS-GFP* in WT and *coi1-2* after root tip resection. Data represent mean ± SEM of 3 independent experiments with at least 8 technical replicates per genotype. Student's *t*- test, * $P < 0.05$, ** $P < 0.01$.

(G) Representative images of GUS staining of *pERF115::GUS* and *pmERF115::GUS* 6 hours after root tip resection. Nine independent *pERF115::GUS* and nine independent *pmERF115::GUS* lines were analysed separately with consistent results.

(H) RT-qPCR of *ERF109* +/- 50 µM MeJA treatment for 1 hour. Two-millimetre root tips of three-day-old of Col-0 seedlings were harvested for RNA extraction and qRT-PCR analysis. *ERF109* transcript level in Col-0 without JA treatment was arbitrarily set to 1. Data represent mean ± SEM of 3 independent experiments. Lowercase letters indicate statistically different groups (Student's *t*- test, $P < 0.01$).

(I and I') GUS staining and confocal image of *pERF109::GUS* 60 min after ablation. Images display the same root for I and I'.

(J) GUS staining of *pERF109::GUS* after root-tip resection at the indicated time points.

(K) GUS staining of *pERF109::GUS* with low and high cut at 90 min after resection.

(L and M) Confocal images of *pERF115::GUS-GFP* and *ERF109-SRDX pERF115::GUS-GFP* +/- 50 µM MeJA treatment for 4 hours. *ERF109-SRDX*, *35S::ERF109-SRDX*. n>10.

(N-P) GUS staining of the indicated genotypes at 90 min after resection. n>7.

(Q) Quantification of new columella cell layers between QC and ablated cells after QC ablation in indicated genotypes. Data represent mean ± SEM of 2 independent experiments.

(R) Meristem length of *pWOX5::GFP* and *pWOX5::GFP erf109* at 3 DAG. Meristem length was measured from root tip until the first elongated cortical cell. Error bars represent SD (n=15). Same lowercase letters indicate no statistical difference (Student's *t*- test, $P < 0.05$).

(S) Meristem length of *pWOX5::GFP* and *pWOX5::GFP coi1-1* at 3 DAG. Error bars represent SD (n=12). Same lowercase letters indicate no statistical difference (Student's *t*-

test, P < 0.05).

(T) Quantification of the frequency of regeneration in Col-0, *erf115* and *ERF115-SRDX*. Data represent mean ± SEM of 3 independent experiments with at least 20 technical replicates per genotype.

(U) Meristem length of Col-0, *erf115* and *ERF115-SRDX* at 3 DAG. Error bars represent SD (n=12). Lowercase letters indicate statistically different groups (Student's *t*- test, P < 0.05). Scale bars, 50 µm.

Supplemental figure 6 **Synergy between JA and auxin signaling in regulating regeneration. Related to Figure 6.**

(A) GUS staining of *pERF109::GUS* with mock treatment, IAA 1 µM, MeJA 50 µM, or IAA 1 µM + MeJA 50 µM for 4 hours, respectively.

(B) RT-qPCR analysis of *ERF109* transcript with mock treatment, IAA, MeJA, or IAA+MeJA with indicated concentrations for 4 hours, respectively. Data represent mean ± SEM of 3 independent experiments. Lowercase letters indicate statistically different groups (Tukey's test, P < 0.05).

(C) Quantification of *CYCD6;1-GFP* fluorescence +/- MeJA treatment. Data represent mean ± SEM. Lowercase letters indicate statistically different groups (Student's *t*- test, P < 0.01).

(D and E) Time course of the expression of *pCYCD6;1::GUS-GFP* after root tip resection. Images display same root for D, and same root for E. White arrow marks ectopic expression of *CYCD6;1* in vascular cells. Scale bar, 50 µm.

(F) ChIP-qPCR of ERF109 on the promoter of *CYCD6;1*. The ChIP signal was quantified as the percentage of total input DNA by qPCR, and normalized to the signal of Col-0 IR fragment (set as 1). The fragment of *ASA1* promoter (Cai et al., 2014) was used as a positive control. Data represent mean ± SEM of 3 independent experiments. IR, intergenic region. (Student's *t*- test, *P < 0.05, **P < 0.01).

(G and H) Confocal images of *pCYCD6;1::GUS-GFP* and *ERF109-SRDX pCYCD6;1::GUS-GFP* +/- 500 nM MeJA treatment for 16 hours. n>15.

(I) Quantification of new columella cell layers between QC and ablated cells after QC ablation in Col-0 and *cycd6;1*. Data represent mean ± SEM of 2 independent experiments.

(J) Meristem length of Col-0 and *cycd6;1* at 3 DAG. Error bars represent SD (n=8). Same lowercase letters indicate no statistically different groups (Student's *t*- test, P < 0.05).

Supplemental figure 7 **JA mediated wounding response and tissue regeneration is important to accommodate soil penetration and parasitic pressures. Related to Figure 7.**

(A) Camera images of plants growing on the 1/2 GM plate and sand plate. Scale bar, 1 cm.

(B) Fluorescence ratio of *JAS9-VENUS*/*H2B-RFP* in WT and *coi1-2* background growing on 1/2 GM plate or sand, respectively. Bars represent SE, n=6 (1/2 GM); n=12 (sand). Student's *t*- test, ****P* < 0.001.

(C) Expression of *JAS9-VENUS* on 1/2 GM plate or on sand plate for 5 min, n=8. Scale bar, 100 µm.

(D-G) Confocal images of *JAS9-VENUS* +/- nematode (*M. incognita*) infection at different stages. Dashed white lines depicted nematodes. Scale bar, 100 µm.

(H-J) GUS staining of *pERF109::GUS* (H), *pERF115::GUS-GFP* (I) and *pCYCD6;1::GUS-GFP* (J) +/- nematode infection at different stages.. Scale bars, 50 µm.

(K) Average number of galls per root tip in the indicated lines at 7-week post infection. Data represent mean ± SEM of 3 independent experiments with 6 replicates per genotype. Lowercase letters indicate statistically different groups. Tukey's test, *P* < 0.01.

(L) Expression of *pCYCD6;1::GUS-GFP* in WT and *ERF115-SRDX* background at 5 DAG. Scale bar, 50 µm

CONTACT FOR REAGENT AND RESOURCE SHARING

Further information and requests for resources and reagents should be directed to and will be fulfilled by the Lead Contact, Ben Scheres (ben.scheres@wur.nl).

EXPERIMENTAL MODEL AND SUBJECT DETAILS

Plants

Arabidopsis thaliana ecotype Col-0 was used as wild type control. Seeds were surface-sterilized for 15 min in 20% commercial bleach, washed five times with sterile water, and plated on 1/2 MS medium with 1% sucrose and 0.8% agar. Plants were stratified at 4°C for 2 days in the dark and then transferred to a phytotron at 22°C with a 16 h light/8 h dark photoperiod (light intensity: 120 µmol photons $m^{-2}s^{-1}$) in oriented Petri dishes. The *myc2* mutant was selected by its reduced root growth inhibition (compared to WT) on MeJA plates, and was confirmed with PCR genotyping. *coi1-1* and *coi1-2* mutants were selected by their reduced root growth inhibition and reduced anthocyanin accumulation (compared to WT) on MeJA plates. For genotypes observed in F1, phenotypes were compared to control F1s (parent X Col-0).

Nematodes

The *Meloidogyne incognita* strain Morelos (from INRA, Sophia Antipolis, France) was used for infection. Eggs of *M. incognita* were obtained as reported (Warmerdam et al., 2018). In brief, eggs were collected on a 25 µm sieve and incubated in sterile tap water containing 1.5 mg ml^{-1} gentamycin and 0.05 mg ml^{-1} nystatin in the dark at room temperature. Hatched juveniles were collected after 4 days and surface sterilized (0.16mM $HgCl_2$, 0.49mM NaN_3, 0.002% (v/v) Triton X-100) for 10 min. After surface sterilization, juveniles were rinsed three times with sterile tap water and transferred to 0.7% Gelrite solution (Duchefa Biochemie, Haarlem, the Netherland).

METHOD DETAILS

Plasmid Construction and Plant Transformation

pERF115::GUS and *pmERF115::GUS* were constructed by fusing a 2400 bp *ERF115* promoter fragment (original or mutated) in front of β-glucuronidase (GUS) in the pGWB3 vector (Nakagawa et al., 2007). *pERF109::GFP* was constructed by fusing a 2935 bp *ERF109* promoter fragment in front of GFP in the pGWB4 vector (Nakagawa et al., 2007). Constructs were transformed into *Agrobacterium tumefaciens* strain C58(*pMP90*) and transformed in plants by floral dip. Transformants were selected based on resistance. Homozygous T3 or T4 transgenic plants were used for analysis.

Histology and Microscopy

Histochemical staining for β-glucuronidase (GUS) activity in transgenic plants was performed as described previously (Chen et al., 2011). In brief, whole seedlings were immersed in GUS staining solution (1 mM X-glucuronide in 100 mM sodium phosphate, pH 7.2, 0.5 mM ferricyanide, 0.5 mM ferrocyanide, and 0.1% Triton X-100) and incubated at 37°C in the dark. Differential interference contrast (DIC) images were captured using a Zeiss photomicroscope III. Modified pseudo-Schiff propidium iodide (mPS-PI) staining: Samples were fixed (10% acetic acid, 50% methanol) and kept at 4℃ for overnight, rinsed briefly with water, and incubated in 1% periodic acid (an oxidizing agent) for 40 minutes-1 hour. After that, samples were washed with water and incubated in Schiff reagent with propidium iodide (100 mM sodium metabisulphite; 0.15 N HCl; 100 ug/mL PI) for 2 hours before imaging. SCRI Renaissance 2200 staining: Samples were fixed in SR2200 Staining Solution (0.1% (v/v) SR2200, 1% (v/v) DMSO, 0.05% (w/v) Triton-X100, 5% (w/v) glycerol, 4% (w/v) para-formaldehyde in PBS buffer (pH 8.0)) and kept at 4℃ for overnight before imaging. For confocal laser scanning microscopy, the root tips were stained in 10 μg/mL propidium iodide and observed using a Zeiss LSM 710 system. 3 DAG seedlings were transferred to 1/2 GM (germination medium) +/- MeJA 48 hours before QC division quantification. PI was visualized using wavelengths of 600–640 nm. Wavelengths used to visualize GFP and YFP were 500–540 and 525–565 nm, respectively. Images were taken with ZEN 2012 software (Zeiss) and processed with Adobe Photoshop.

RT-qPCR Analysis
Total RNA from whole seedlings or root tips were extracted using the Spectrum Plant total RNA Kit (Sigma). For MeJA treatment, seedlings were transferred to plates +/- MeJA for indicated time courses before harvest. cDNA was synthesized from 5 μg total RNA using odT18VN primer (Biolegio) and RevertAid M-MuLV reverse transcriptase (Fermentas). qPCR reactions were quantified on a Bio-Rad CFX connect Real-time System with iQ SYBR Green Supermix (Bio-Rad). Expression levels of tested genes were normalized against *ACT2*. Primers are listed in Table S1.

Laser Ablation and Resection
Laser ablations were performed on a Leica TCS SP8 confocal microscope (software: Leica Application Suite Advanced Fluorescence). 2-to 3- DAG seedlings were used, and ablation procedures were performed as previously described (Xu et al., 2006). For MeJA treatment, seedlings were transferred to plates +/- MeJA for the indicated time course. At least three independent experiments were performed. For quantification of *JAS9-VENUS* JA biosensor fluorescence with or without QC ablation, at least 5 nuclei in lateral root cap/epidermis near ablated QC were traced and quantified during the time course in each root tip. Mocks are seedlings mounted on slides with PI without laser ablation. Root tip resection experiments were performed as previously described (Sena et al., 2009). All root-tip excisions were performed at 3 DAG. At least three independent experiments were performed.

Nematode Infection Assays
Nematode infection assays on Arabidopsis plants were performed as previously described (Warmerdam et al., 2018). In brief, for egg mass number count, Arabidopsis seeds of different genotypes were vapor sterilized and planted in 6-well cell culture plates (Greiner bio-one) containing MS medium (MS with vitamins 4.7 g/L (Duchefa biochemie), 58.5 mM sucrose and 5 g/L Gelrite. After at least 3 days of stratification in the dark at 4°C, plants were grown at 24 degrees under 16-h-light/8-h-dark. Each two-week-old seedling was inoculated with ~180 surface sterilized J2s of *Meloidogyne incognita* (Strain Morelos) and plants were incubated at 24 degrees in the dark. The number of egg masses per plant was counted seven weeks after inoculation by visually inspecting the roots with a stereomicroscope (ZEISS Stemi SV6). For the root recovery measurements, vapor sterilized Arabidopsis seeds were planted in two rows on square plates (120x120x15mm, Greiner bio-one) containing MS medium (MS with vitamins 4.7 g/L (Duchefa biochemie), 58.5 mM sucrose and 7 g/L Gelrite. After stratification, seedlings were vertically grown at 24 degrees under 16-h-light/8-h-dark for 4 days until inoculation with ~25 surface sterilized J2s of *Meloidogyne incognita* (Strain Morelos) or mock inoculation. The positions of the root tips of the primary roots at the time of inoculation were marked on the plates as a reference point for further growth. Growth of the primary root relative to this marker position was measured from 2 dpi to 6 dpi for nematode- and uninfected roots. Nematode-

infected roots were identified by the formation of a gall at the marker position. WinRHIZO Software and EPSON STD4800 were used to scan each genotype. For counting root tips, seedlings were grown vertically on square plates using the same media and growth conditions as for the above-described nematode infection assays. The counting of root tips was performed 4 days after plants were incubated at 24 degrees in the dark. For marker gene expression after nematode infection, seedlings were grown vertically on square plates containing nematode infection medium. Four-day-old seedlings were inoculated without (control) or with surface sterilized J2s of *M. incognita* and were incubated at 24 degrees in the dark. One to three days after nematode inoculation, seedlings were analyzed under confocal microscopy (Zeiss LSM 710), or were used for GUS/EdU staining. The statistical significance of the pairwise differences between plant genotypes was assessed with a one-way ANOVA.

Rhizotrons

We mixed sterilized river sand (Van Leusden Transport, Wageningen, the Netherlands) (diameter 250 µm-1 mm (>98%), 1 mm-10 mm (<2%)), Agra-perlite (Grain 2.0-3.0 mm) and clay granules (diameter ~3 mm) (Seramis®) (volume: 8:1:1) and filled square petri dishes (greiner bio-one, 120x120x17 mm). Rhizotrons were pre-wetted with sterilized 1/2 MS liquid. For marker gene expression observation, young seedlings were grown on 1/2 GM plates for 4-5 days, and were transferred to new plates or sand plates for another 4 days. For primary root length measurement, seedlings were grown on 1/2 GM plates for 4 days, and then were transferred to new plates or sand plates for another 3 days before measurement. Thereafter, rhizotron sand mixtures were carefully washed with milliQ water and seedlings were placed on new 1/2 GM plates before imaging or root length measurement. For marker gene expression, images were taken with identical confocal settings. Three independent experiments were performed for both primary root measurement and marker gene expression. In each independent experiment, at least 16 roots per genotype were measured for primary root length, and at least 10 roots were visualized for marker gene expression per genotype. ImageJ and the SmartRoot plugin were used for primary root length measurements.

Luciferase Assay

Promoter activity was measured using a Dual Luciferase Reporter (DLR) system (Promega). In brief, *pCYCD6;1::LUC* and p19 (gene-silencing supressor) constructs were co-tranformed with the appropriate transcription factor constructs into three weeks old tobacco leaves. *35S:Renilla*-luciferase (rLUC) was used as an internal control to quantify transformation efficiency. Three days after inoculation, proteins were extracted with Dual-Luciferase Reporter Assay System kit (Promega, Fitchburg, USA). Luciferase activity measurements were performed with Glomax™ 96 microplate luminometer (Promega, Fitchburg, USA). The measured levels were normalized using rLUC values and the ratio was calculated relative to the ones obtained from leaves transfected with only *pCYCD6;1::LUC*.

ChIP-qPCR Assay

ChIP experiments were performed as described (Li et al., 2017). In brief, approximately 1 gram of wild-type Col-0 (control) and *35s::MYC2-GFP* seedlings at 5 DAG were used for each anti-GFP ChIP assay. Samples were treated with MeJA 100 µM for 2 hours before harvest. Sonicated chromatin was incubated with GFP-Trap agarose beads (Chromotek) for overnight at 4 degrees. Precipitated DNA was purified using a ChIP DNA clean & concentrator kit (The epigenetics company) for RT-qPCR analysis. Sonicated chromatin of *35S::HA-ERF109* was incubated was anti-HA antibody (abcam) and Dynabeads protein G. Three independent ChIP experiments were performed. Primers used for ChIP-PCR are listed in Table S1.

Y2H, BiFC and Co-IP Assays

Y2H, BiFC and Co-IP were performed as described (Gehl et al., 2009; Shimotohno et al., 2018; Zhang et al., 2018). *N. benthamiana* leaves were used for BiFC and Co-IP experiments. In Co-IP experiment, protein A/G plus agarose beads (Santa Cruz Biotechnology) were added to protein extracts to reduce nonspecific immunoglobulin binding prior to antibody incubation. The LxCxE motif in the ERF115 CDS was mutated with the quikchange II XL site-directed mutagenesis kit (Agilent). Primers used are listed in Table S1.

QUANTIFICATION AND STATISTICAL ANALYSIS

Detailed statistical parameters of the experiments can be found in figure legends (type of statistical tests used, exact value of n, etc). In figures, asterisks denote statistical significance between samples/treatments. Statistical significance was evaluated by Student's *t* test analysis. For multiple comparisons, an analysis of variance followed by Fisher's LSD mean separation test and Turkey's HSD test (SPSS) was performed on the data. Samples marked with different lowercase letters are statistically different at $P < 0.01$ or $P < 0.05$, as indicated in figure legends. Data presented are mean values of at least three biological repeats with SD or SE. For sand/soil root growth and nematode infection assays, seedlings were photographed and root length was measured (Image J). QC cell numbers were analyzed on confocal images (ZEN 2012, Zeiss) as previously described (Chen et al., 2011). Images were processed with Adobe Photoshop and Adobe Illustrator.

Supplementary Table 1 List of primers used in this study

CellPress

TABLE FOR AUTHOR TO COMPLETE

Please upload the completed table as a separate document. ***Please do not add subheadings to the Key Resources Table.*** *If you wish to make an entry that does not fall into one of the subheadings below, please contact your handling editor. (**NOTE:** For authors publishing in Current Biology, please note that references within the KRT should be in numbered style, rather than Harvard.)*

KEY RESOURCES TABLE

REAGENT or RESOURCE	SOURCE	IDENTIFIER
Antibodies		
Roche anti-GFP mouse IgG1k antibody	Roche	Cat#11814460001; RRID:AB_390913
c-Myc (9E10) antibody	Santa Cruz Biotechnology	Cat# sc-40; RRID:AB_627268
c-Myc (9E10) antibody conjugated to agarose	Santa Cruz Biotechnology	Cat# sc-40AC;
Rabbit anti-HA tag polyclonal antibody	Abcam	Abcam Cat# ab9110, RRID:AB_307019
GFP-Trap magnetic agarose beads	Chromotek	Cat# gtma-10
Goat anti-mouse IgG-HRP Polyclonal, HRP Conjugated antibody	Santa Cruz Biotechnology	Cat# sc-2005, RRID:AB_631736
Chemicals, Peptides, and Recombinant Proteins		
Propidium Iodide (PI)	Sigma-Aldrich	Cat# P4170
SCRI Renaissance 2200 (SR2200)	Renaissance Chemicals	N/A
Methyl jasmonate 95% (MeJA)	Sigma-Aldrich	Cat# 392707
Indole-3-Acetic Acid (IAA)	Duchefa	Cat# I0901.0100
Hydrogen peroxide 30%	Merck	Cat# 1072091000
Dynabeads protein G for immunoprecipitation	ThermoFisher	Cat# 10003D
Protein A/G plus-agarose	Santa Cruz Biotechnology	Cat# sc-2003
Critical Commercial Assays		
Click-iT EdU Alexa Fluor 555 HCS Assay	ThermoFisher	Cat# C10352
Spectrum Plant total RNA Kit	Sigma-Aldrich	Cat# STRN250-1KT
Dual-Luciferase Reporter Assay System	Promega	Cat# E1910
Experimental Models: Organisms/Strains		
Arabidopsis: pSCR::SCRaca:YFP scr-4 (Resistance: pptR)	Cruz-Ramirez et al., 2012	N/A
Arabidopsis: pWOX5::amiGO-RBR (KanR)	Cruz-Ramirez et al., 2013	N/A
Arabidopsis: pWOX5::GFP (pptR)	Blilou et al., 2005	N/A
Arabidopsis: ERF115-OE (KanR)	Heyman et al., 2013	N/A
Arabidopsis: ERF115-SRDX (KanR)	Heyman et al., 2013	N/A
Arabidopsis: ERF115-OE pWOX5::GUS-GFP (KanR)	Heyman et al., 2016	N/A
Arabidopsis: ERF115-SRDX pWOX5::GUS-GFP (KanR)	Heyman et al., 2016	N/A
Arabidopsis: pERF115::GUS-GFP (KanR)	Heyman et al., 2013	N/A
Arabidopsis: pERF115::GUS (HygR)	This paper	N/A
Arabidopsis: pmERF115::GUS (HygR)	This paper	N/A
Arabidopsis: coi1-2	Xu et al., 2002	N/A
Arabidopsis: coi1-1	Xie et al., 1998	N/A
Arabidopsis: 35S::MYC2-GFP (HygR)	Chen et al., 2012	N/A

Arabidopsis: pERF109::GUS (pptR)	Cai et al., 2014	N/A
Arabidopsis: 35S::HA-ERF109 (pptR)	Cai et al., 2014	N/A
Arabidopsis: JAS9-VENUS (HygR)	Larrieu et al., 2015	N/A
Arabidopsis: erf115	SALK	*SALK_021981*
Arabidopsis: erf109	SALK	*SALK_150614*
Arabidopsis: pCYCD6;1::GUS-GFP (KanR)	Sozzani et al., 2010	
Arabidopsis: cycd6;1	GABI-Kat	GK-368E07
Arabidopsis: cycd2;1 cycd6;1	Sozzani et al., 2010	N/A
Arabidopsis: myc2-2	Boter et al., 2004	N/A
Arabidopsis: myc234	Fernández-Calvo et al., 2011	N/A
Oligonucleotides		
Primers used in this study, see Table S1	This paper	N/A
Recombinant DNA		
Plasmid: *pERF115::GUS*	This paper	N/A
Plasmid: *pmERF115::GUS*	This paper	N/A
Plasmid: *ERF109-SRDX*	This paper	N/A
Plasmid: *ERF115-SRDX*	This paper	N/A

Figure 1

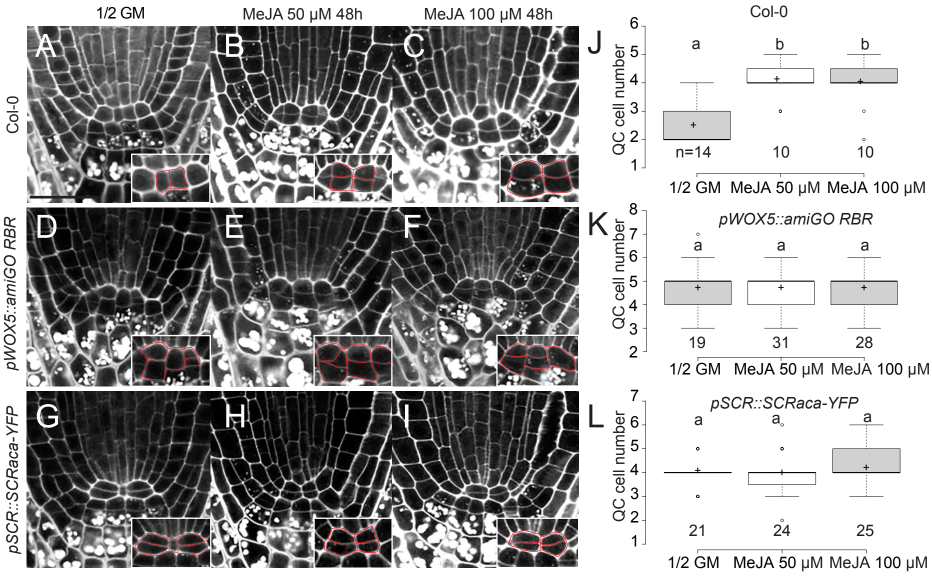

Figure 1. JA acts through RBR-SCR to regulate QC quiescence.

Figure 2 Click here to access/download;Figure;Figure 2.pdf

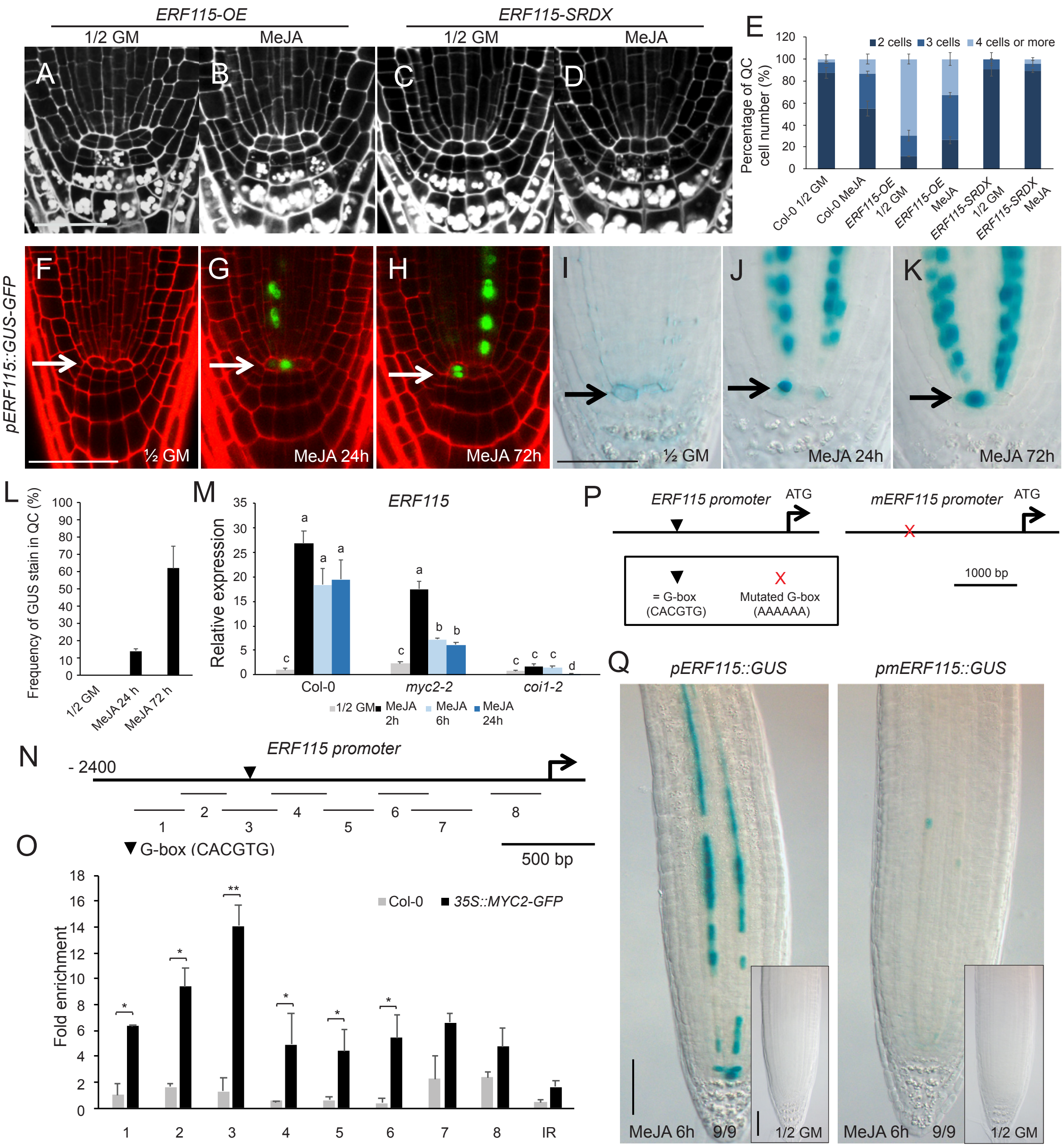

Figure 2. JA induces *ERF115* transcription

Figure 3

Click here to access/download;Figure;Figure 3.pdf

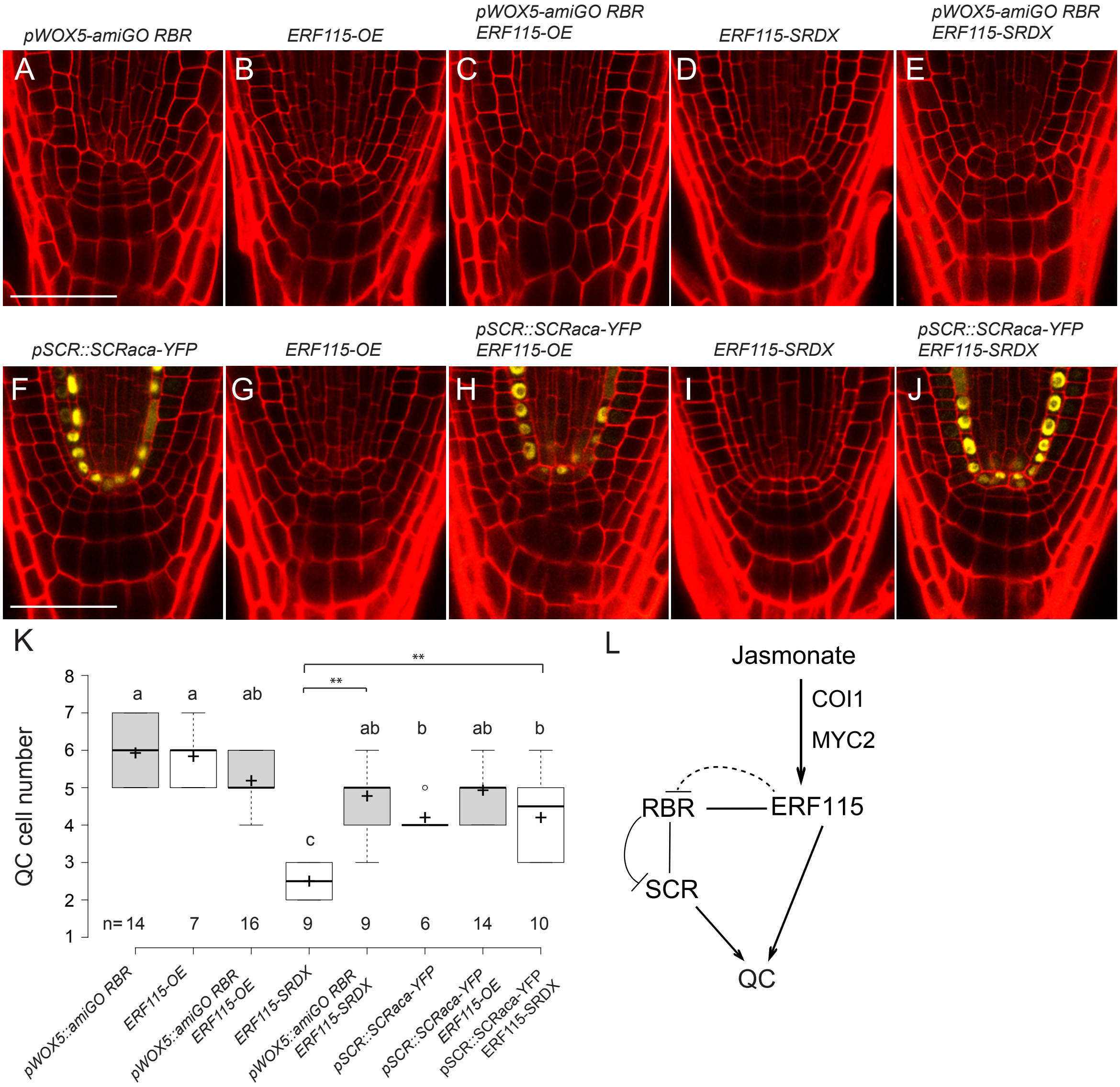

Figure 3 Genetic interaction between RBR-SCR and ERF115

Figure 4 Click here to access/download;Figure;Figure 4.pdf

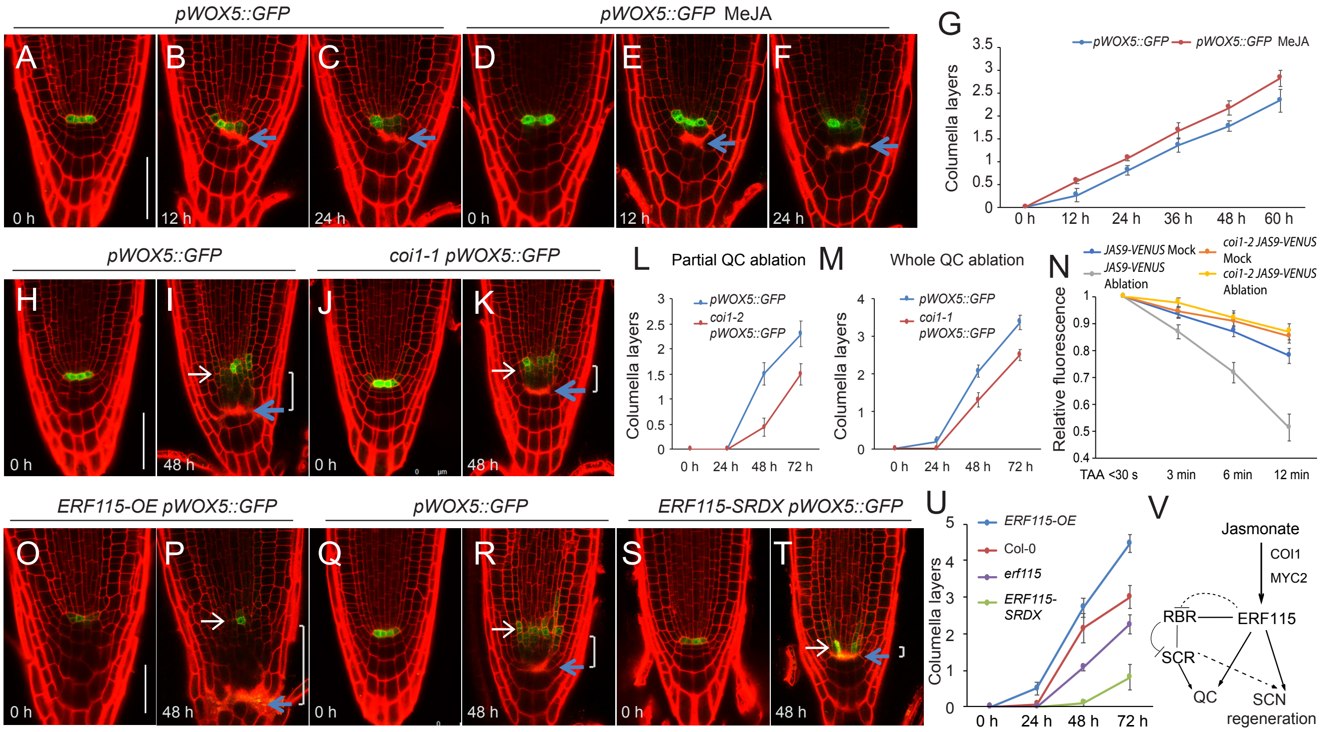

Figure 4 JA signaling promotes stem cell niche regeneration.

Figure 5 Click here to access/download;Figure;Figure 5.pdf

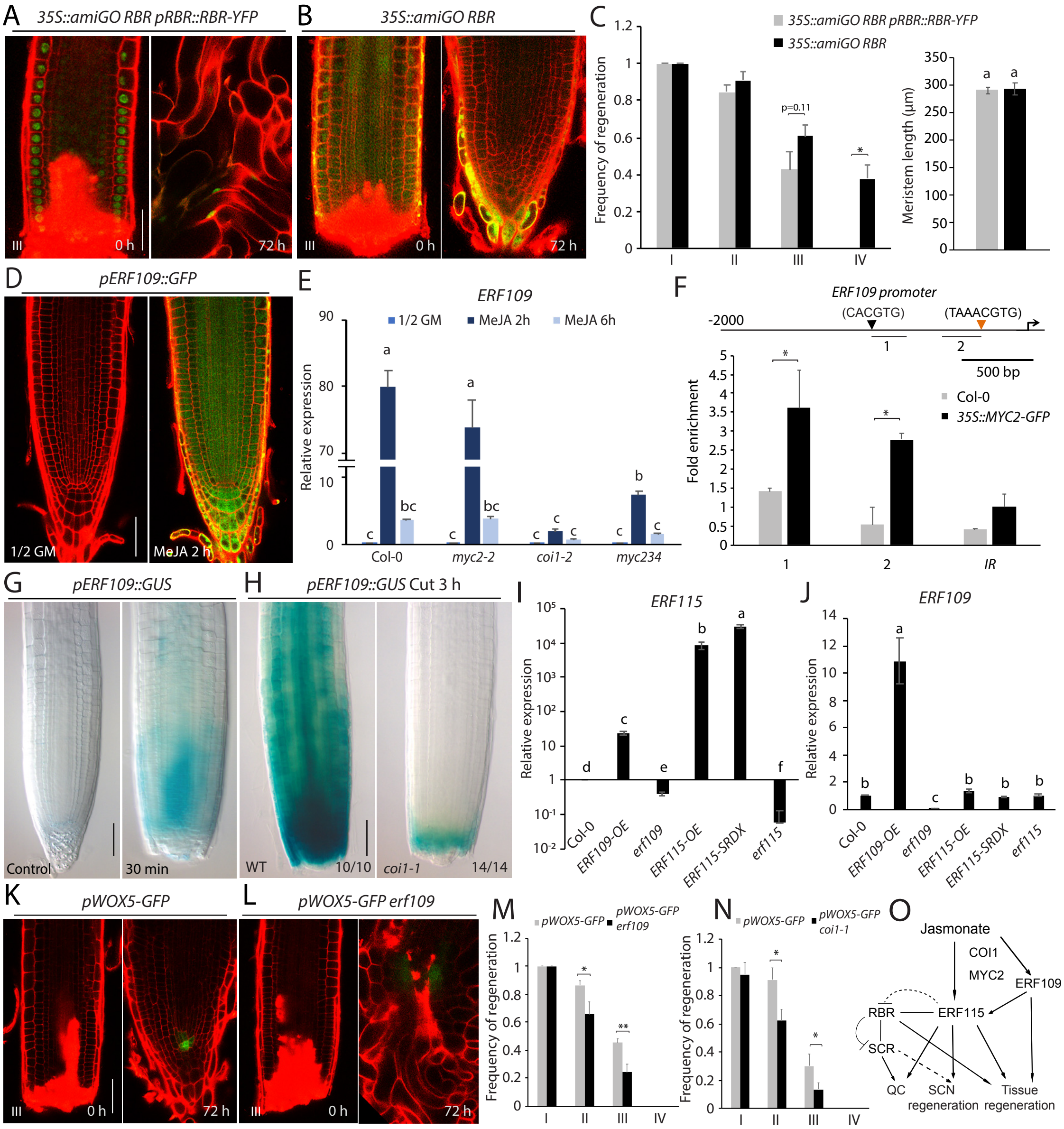

Figure 5 ERF109 responds quickly to JA and wounding, and is required for tissue regeneration.

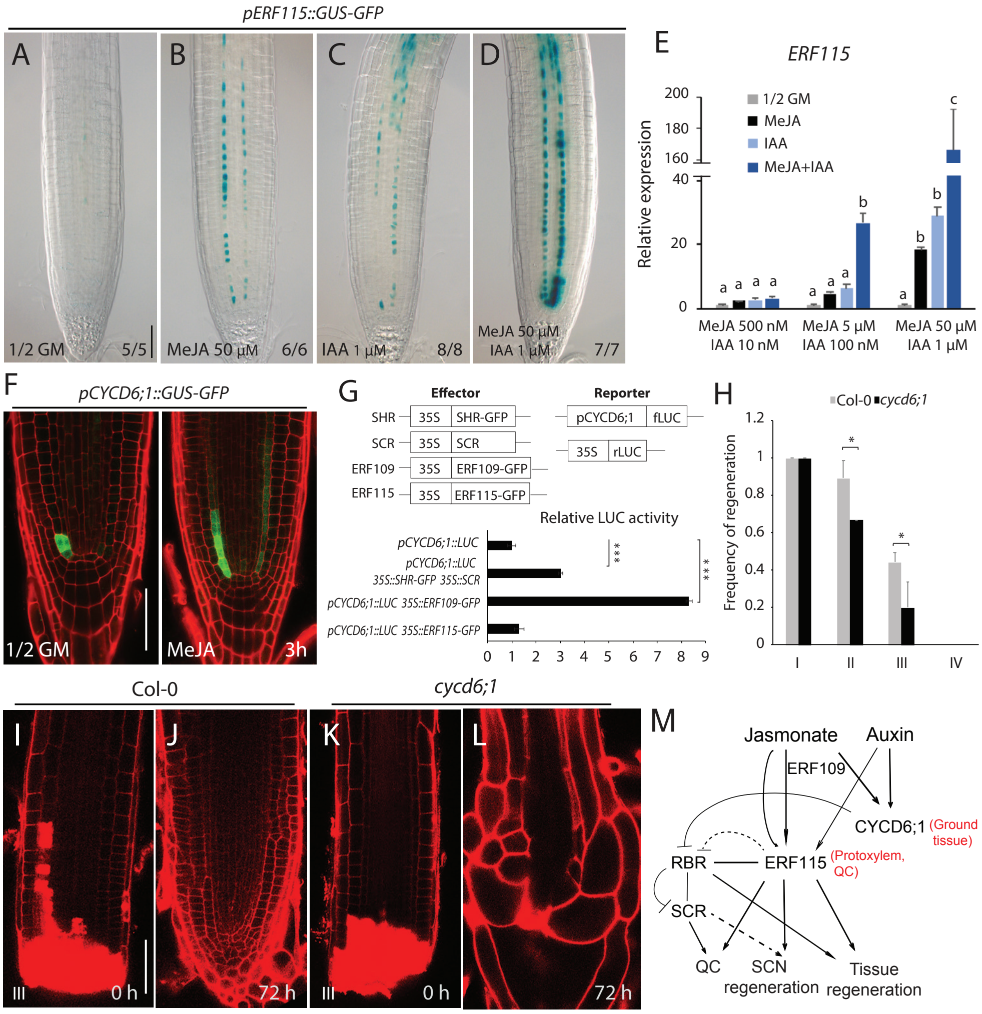

Figure 6. Synergy between JA and auxin signaling in regulating regeneration.

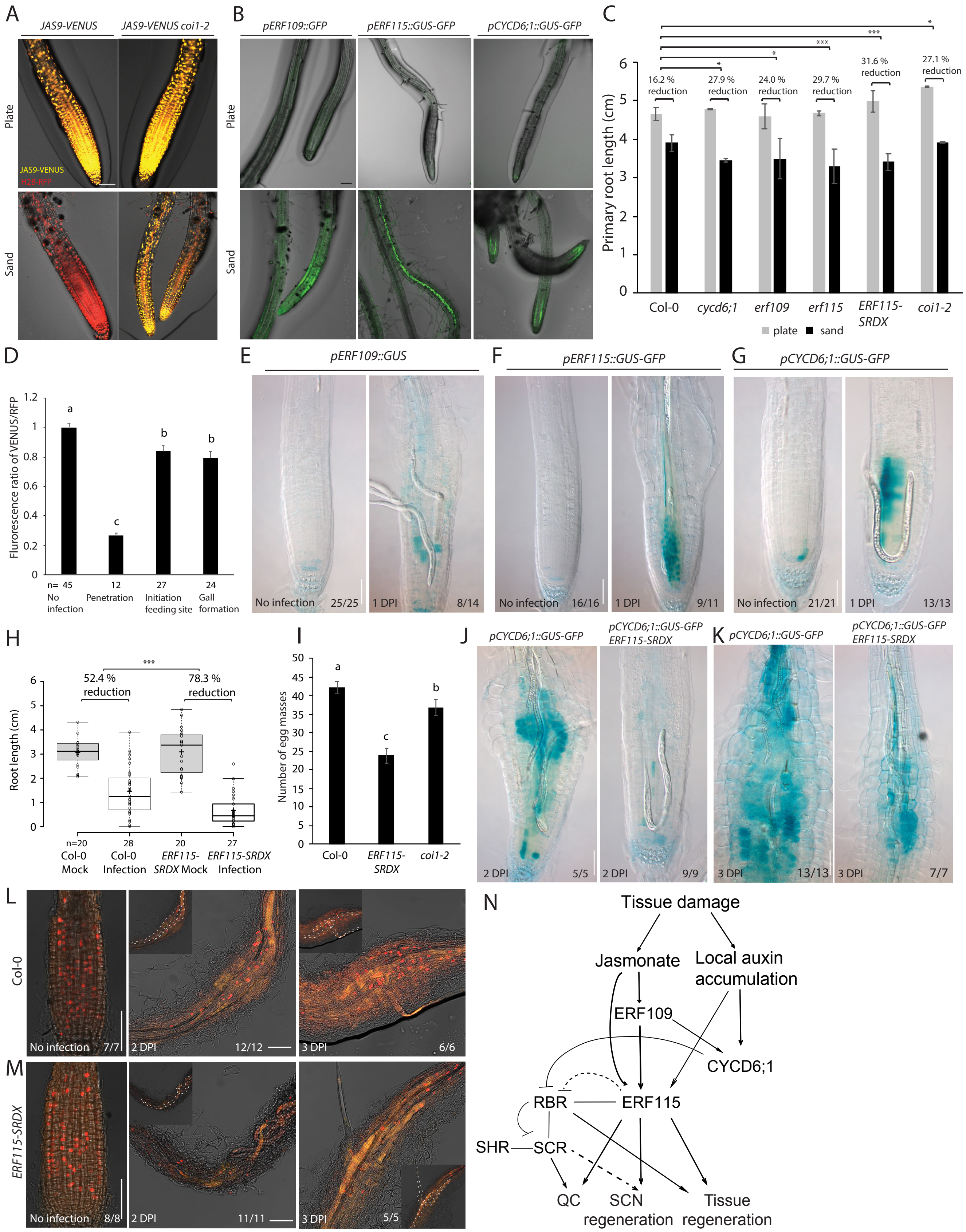

Figure 7 JA mediated wounding response and tissue regeneration is important to accommodate soil penetration and parasitic pressure.